
Article:
Grey, William George orcid.org/0000-0001-8209-5645, Rio-Machin, Ana, Casado, Pedro et al. (11 more authors) (2022) CKS1 inhibition depletes leukemic stem cells and protects healthy hematopoietic stem cells in acute myeloid leukemia. Science Translational Medicine. eabn3248. ISSN: 1946-6242

https://doi.org/10.1126/scitranslmed.abn3248

Title: CKS1 inhibition depletes leukemic stem cells and protects healthy hematopoietic stem cells in acute myeloid leukemia

Authors: William Grey[1,2*], Ana Rio-Machin[3], Pedro Casado[4], Eva Grönroos[5], Sara Ali[1], Juho J. Miettinen[6], Findlay Bewicke-Copley[3], Alun Parsons[6], Caroline A. Heckman[6], Charles Swanton[5,7], Pedro R. Cutillas[4], John Gribben[8], Jude Fitzgibbon[3], Dominique Bonnet.[1*]

Affiliations:

1. Haematopoietic Stem Cell Laboratory, The Francis Crick Institute, London, NW1 1AT, U.K.
2. York Biomedical Research Institute, Department of Biology, University of York, York, YO10 5DD, U.K.
3. Centre for Genomics and Computational Biology, Bart's Cancer Institute, Queen Mary University of London, London, EC1M 6BQ, U.K.
4. Cell signalling and proteomics group, Centre for Genomics and Computational Biology, Barts Cancer Institute, Queen Mary University of London, London, EC1M 6BQ, U.K.
5. Cancer evolution and genome instability laboratory, The Francis Crick Institute, London, NW1 1AT, U.K.
6. Institute for Molecular Medicine Finland – FIMM, HiLIFE – Helsinki Institute of Life Science, iCAN Digital Precision Cancer Medicine Flagship, University of Helsinki, Helsinki, Finland.
7. UCL Cancer Institute, 72 Huntley St, London WC1E 6DD.
8. Centre for Haemato-Oncology, Bart's Cancer Institute, Queen Mary University of London, London, EC1M 6BQ, U.K.

* Corresponding authors: dominique.bonnet@crick.ac.uk, william.grey@york.ac.uk

Single Sentence Summary: Targeting CKS1 has opposing effects in normal and malignant hematopoiesis, protecting normal HSCs while reducing the leukemic stem cell pool.

Abstract

Acute myeloid leukemia (AML) is an aggressive hematological disorder comprising a hierarchy of quiescent leukemic stem cells (LSCs) and proliferating blasts with limited self-renewal ability. AML has a dismal prognosis, with extremely low two-year survival rates in the poorest cytogenetic risk patients, primarily due to the failure of intensive chemotherapy protocols to deplete LSCs, and toxicity of therapy towards healthy hematopoietic cells. We studied the role of CKS1-dependent protein degradation in primary human AML and healthy hematopoiesis xenograft models in vivo. Using a small molecule inhibitor (CKS1i), we demonstrate a dual role for CKS1-dependent protein degradation in reducing AML blasts in vivo, and importantly depleting LSCs, whilst inhibition of CKS1 has the opposite effect on normal hematopoiesis, protecting normal hematopoietic stem cells from chemotherapeutic toxicity. Proteomic analysis of responses to CKS1i demonstrate that inhibition of CKS1 in AML leads to hyperactivation of RAC1 and accumulation of lethal reactive oxygen species, whereas healthy hematopoietic cells enter quiescence in response to CKS1i, protecting hematopoietic stem cells. Together these findings demonstrate CKS1-dependent proteostasis is a key vulnerability in malignant stem cell biology.

Main Text

Introduction

Acute myeloid leukemia (AML) is a heterogeneous, aggressive disease of the hematopoietic system, arising from hematopoietic stem/progenitor cells. The average two-year survival rate is 5-15% in poor risk, older patients with AML patients (>65yr), demonstrating an unmet critical need for new therapeutic approaches*(1)*. Fundamentally, leukemic stem cells (LSCs), the cancer stem cells (CSCs) of the hematopoietic system, are the origins of relapse in AML*(2)* and show substantial plasticity from *de novo* disease through to relapse*(3)*. Therefore, new approaches targeting AML LSCs are critical for improving AML prognosis. Recent developments, such as targeting the anti-apoptotic protein BCL2 using Venetoclax, have demonstrated that therapies affecting protein networks hold great promise for a wide variety of cancers, including poor risk classification patients with AML*(4, 5)*. Yet resistance still emerges through LSC adaptations*(6, 7)*.

The key aim of CSC-targeted therapy is to selectively reduce CSCs without negatively affecting normal stem cells. Improved understanding of the biological differences between normal and malignant stem cells is needed to achieve selective CSC targeting, without toxicity to normal stem cells.

We previously reported a regulatory axis between the cyclin-dependent kinase (CDK) subunits Cks1 and Cks2, and the mixed lineage leukemia 1 protein (Mll1). Mll1 is a key protein hijacked during neoplastic transformation of the hematopoietic system*(8)* and important for regulation of normal and cancer stem cells from multiple different tissues*(9, 10)*. Cks1 and Cks2 have multifaceted overlapping and independent roles in balancing protein homeostasis, so called "proteostasis", throughout the cell cycle, ensuring correct G0/G1 transition*(11)*, chromatin separation*(12–14)* and DNA repair*(11, 15, 16)*. Cks1 and Cks2 also possess CDK-independent functions, in concert with the Skp1/2, cullin, F-box containing complex (SCF^{SKP2}) and anaphase promoting complex (APC^{CDC20}) E3 ubiquitin ligases, important for selective protein degradation*(11, 12, 17)*.

The ubiquitin proteosome system (UPS) is a highly regulated system that controls protein degradation and is essential for correct cellular protein homeostasis. It has been reported that up to 80% of cellular proteins are degraded by the UPS, demonstrating its importance in proliferation, survival, differentiation and drug resistance *(18–21)*. Targeting the UPS has proved elusive in hematopoietic disorders. Broad spectrum inhibitors of protein degradation, such as Bortezomib, have shown increased toxicity without improvement of overall survival *(22)*. Targeting less broad cullin-dependent protein degradation, using drugs such as Pevonedistat, was initially promising *(23, 24)*, but trials have failed to significantly improve overall survival*(25*). We previously demonstrated in vitro that pan-cullin inhibition can lead to cell cycle arrest in AML, whereas more specific inhibition of protein degradation targeting CKS1 leads to cell death *(8)*. Indeed, small molecule inhibitors targeting SCF-SKP2-CKS1 are able to stabilise p27 protein and block cancer cells in G2/M phase of the cell cycle, leading to cell death, rather than cell cycle arrest *(8, 26, 27)*.

In the current study, we investigated the sensitivity of poor risk AML – a sub-classification with few treatment options – to protein phosphorylation and degradation inhibitors to reveal CKS1-dependent vulnerabilities. We demonstrate efficacy in reducing the LSC pool through the inhibition of CKS1-dependent protein degradation either as a single treatment or in combination with standard chemotherapy. In contrast,

CKS1 inhibition had the opposite effect on normal hematopoiesis, improving stem cell functionality and conferring protection from chemotherapeutic toxicity. Together, these findings offer a new treatment for eradicating drug resistant LSCs whilst preserving healthy hematopoiesis.

Results

High expression of *CKS1B* dictates sensitivity of bulk AML to inhibition of CKS1-dependent protein degradation

The overexpression of *CKS1B* correlates with poor prognosis in a variety of solid tumors*(28–30)*, but is an indeterminant factor in AML (Fig. S1A-D) despite a broad range of expression in normal and malignant hematopoiesis across multiple cohorts and datasets (Fig. S1E). *CKS1B* expression varied significantly between both normal and malignant hematopoiesis and within different hematopoietic subtypes (Kruksal-Wallis, $P<2.2^{-16}$, Supp. Table S1), with intermediate expression in healthy hematopoietic stem cells (HSCs), and a broad range of expression in most AML cytogenetic subtypes compared to one of its key upstream proteostatic regulation partners *SKP2* (Fig. S1F).

We hypothesized that high *CKS1B* expression in AML may provide a selective susceptibility to inhibition of either CDK-CKS1-dependent phosphorylation or SCF-CKS1-dependent protein degradation by an $SCF^{SKP2\text{-}CKS1}$ E3 ligase inhibitor, hereafter referred to as CKS1i*(26, 27)*. To address this key question, we screened a cohort of cytogenetically poor risk AMLs, spanning a variety of morphological (French-American-British, FAB) and molecular subtypes, with a broad range of *CKS1B* expression (Figure 1A, Supp. Table S2). AMLs were tested for sensitivity to a range of CDK inhibitors, a broad-spectrum protein degradation inhibitor (Bortezomib), and specific inhibitors of the $SCF^{SKP2\text{-}CKS1}$ E3 ubiquitin ligase complex (Pevonedistat and CKS1i; Figure 1A-B, Fig. S2A-B, Supp. Table S3).

Whilst CDK inhibition resulted in fewer than 50% of primary AML samples demonstrating robust drug sensitivity (DSS), whereas protein degradation inhibitors demonstrated increased drug sensitivity of AML blasts grown in vitro (Fig. S2A). Since failure of broad-spectrum protein degradation inhibitors has been reported previously, and we reported induction of quiescence rather than cell death by Pevonedistat*(8)*, we investigated whether inhibition of more specific CKS1-dependent protein degradation

could be more effective. Indeed, knockdown of *CKS1B* in AML results in dose- and time-dependent reduction in viability (Fig. S2C-E), and CKS1i drug sensitivity directly correlated with *CKS1B* expression in poor risk patients with AML patients (R=0.61, p=0.0078; Figure 1C), with clear separation of high and low DSS (Fig S2F). Separating patients at the 50th percentile by *CKS1B* expression revealed significantly increased drug sensitivity in *CKS1B^{high}* versus *CKS1B^{low}* patients with AML patients (P=0.0035, Fig S2F), indicating that RNA expression of *CKS1B* could be a selection criterion for targeting SCF$^{SKP2\text{-}CKS1}$ dependent protein degradation in AML. Additional characterization of patient phenotypes indicated that white blood counts at diagnosis are similar between patients with *CKS1B^{high}* and *CKS1B^{low}* expressing tumors and CKS1i responders and non-responders, and both groupings covered an array of mutational profiles, with a multivariate analysis demonstrating only *CKS1B* expression correlates with in vitro CKS1i sensitivity (Fig. S2G-I, Supp. Tables S4 , S5 & S6).

In order to investigate the effect of CKS1i on primary patient AML in vivo, we selected five primary patient samples with a range of *CKS1B* expression to engraft in immunodeficient NSG mice (Supp. Table S2). A single course of CKS1i (10mg/kg, 5 days treatment I.P.) significantly reduced the leukemic burden in mice engrafted with patient AMLs carrying the highest *CKS1B* expression (AML12 P=0.001 and AML21 P=0.04). A trend towards reduced AML burden was seen at intermediate level of *CKS1B* expression (AML26), but CKS1 inhibition had no significant effect on bulk AML in mice for patient samples with the lowest *CKS1B* expression (AML27 and AML32; Figure 1D). As such, *CKS1B* expression directly correlated with acute tumor reduction in vivo (R=-0.446; Figure 1E). All CKS1i treated AML xenografts showed a delay in AML bone marrow colonisation over time, regardless of tumor reduction immediately post-CKS1i treatment (Fig. S3) and improved overall survival compared to untreated controls (Figure 1F-J). This indicates that CKS1i treatment had additional effects beyond acutely reducing bulk leukemic burden of *CKS1B^{high}* AML in mice.

CKS1-dependent degradation is a specific vulnerability in leukemic stem cells

Whilst reducing leukemic blast count is the current backbone of clinical chemotherapeutic protocols and required to release leukemic cell-mediated suppression of normal hematopoietic cells, these approaches do not target quiescent LSCs, the subset of cells at the origin of relapse in vivo*(31)*. The observed effect on bone marrow colonisation and overall survival upon CKS1i treatment in *CKS1B*^{low} AML

xenograft mice could indicate a specific mechanism of action of CKS1i on LSCs. Indeed, LSCs are rare and bulk *CKS1B* expression does not account for LSC-specific *CKS1B* dependency.

Transcriptomic analysis of patient AMLs at single cell resolution revealed subsets of AML expressing *CKS1B* clustering with LSC genes (Fig. S4A-B). To better quantify LSC-dependency on CKS1 in primary patient AML, we investigated CKS1 protein abundance at single cell resolution. Mass cytometry-based *t*-stochastic neighbor embedding demonstrated strong association of CKS1 protein abundance with a range of immunophenotypic and functional LSC markers (Figure 2A, Fig. S4C). When focussing on primary patient immunophenotypic LSC subpopulations ($CD200^+CD99^+CLL\text{-}1^+CD123^+CD117^+$, Fig. S5A), CKS1 protein abundance was significantly higher than bulk AML ($P=0.0002$, Figure 2B). Similarly, immunophenotypic LSCs had increased abundance of proteins important for both stem cell functionality and drug resistance, such as BCL2, active β-catenin (Fig. S5B). To assess the functional effect of CKS1i on LSCs we used the leukemic-long-term culture initiating cell assay (L-LTC-IC). All patient samples showed significant reduction in L-LTC-IC frequency, demonstrating a direct effect of CKS1i treatment on LSC functionality ($P<0.0001$, Figure 2C-D, Fig. S5C). In addition, primary human AML cells recovered from AML26 xenografts were secondarily transplanted in limiting dilution. No xenografts carrying previously CKS1i treated AMLs showed overt signs of ill-health, whereas control xenografts died within 150 days (Figure 2E). Analysis of human bone marrow engraftment of secondary xenograft mice demonstrated reduction in LSC frequency by CKS1i treatment (Figure 2F, Fig. S5D). In agreement, when cultured in vitro, patient AML samples treated with CKS1i show increased apoptosis in the LSC compartment (Figure 2G) and a reduction in LSCs compared to total AML blasts (Figure 2H).

These data demonstrate that LSCs have high concentrations of CKS1 and CKS1i is efficient at targeting the LSC compartment. The reduction of LSCs by CKS1i indicates a clear route to combating AML in all patients independent of bulk *CKS1B* expression.

CKS1 inhibition protects healthy hematopoiesis from chemotherapeutic toxicity

Contrary to primary patient AML LSCs and AML cell lines, healthy umbilical cord blood derived $CD34^+$ and the more primitive $CD34^+CD45RA^-$ compartment did not undergo

apoptosis in response to CKS1i (Figure 3A). Where AML cells accumulated in S-G2-M phases of the cell cycle (Fig. S5E), healthy $CD34^+$ cells increased p27 abundance in primitive fractions (Figure 3B) and became significantly more quiescent (P=0.01, Figure 3C), leading to fewer cells in culture over time (Figure 3D).

By inducing quiescence and limiting cell growth, CKS1i would reduce the ability to incorporate nucleotide analogues, such as Cytarabine, and the toxicity of topoisomerase inhibitors, such as Doxorubicin. We hypothesized that this could place CKS1i as a "chemoprotective agent" during classical induction chemotherapy in AML, protecting healthy hematopoietic cells from chemotherapeutic killing.

To investigate this hypothesis, we engrafted healthy umbilical cord blood derived $CD34^+$ cells in NSG mice and treated the mice with the clinical chemotherapy protocol of cytarabine plus doxorubicin (5+3 days)*(33)*, in the presence or absence of CKS1i (Figure 3E). Human bone marrow engraftment increased in untreated control mice between weeks 4 and 6 as expected. Treatment at week 4 with doxorubicin/cytarabine (DA) reduced bone marrow engraftment by week 6, reducing the expansion of human cells compared to control, but addition of CKS1i (DAC) was able to rescue this effect, returning expansion of human cells similar to controls (Figure 3F-G). Better engraftment at week 6 was complemented by a reduction in apoptotic human cells in the bone marrow of recipient mice (Figure 3H-I), indicating that CKS1i treatment prevents DA-induced cell death in normal hematopoietic cells. Secondary transplantation of human cells obtained from primary treatment mice showed an increase in HSC frequency after CKS1i treatment, rescuing DA effects on HSCs (Figure 3J). This indicates that CKS1i protects healthy HSCs from chemotherapy induced depletion.

Outside of the hematopoietic system a key side-effect of induction chemotherapy for AML is severe gut by-toxicity, often resulting in intestinal dysfunction and infection*(34, 35)*. In agreement with the effects on normal HSPCs, DA treatment induced increased proliferation of intestinal crypts (Fig. S6A-B) and resulted in fewer $LGR5^+$ crypts post-chemotherapy (Fig. S6C-D). Both phenotypes were rescued by the addition of CKS1i, returning proliferation and number of $LGR5^+$ crypts to control numbers.

These data demonstrate that CKS1i has the opposite effect on healthy tissue compared to AML, and suppression of growth induced by CKS1i can be chemoprotective for healthy tissue during clinically used chemotherapy.

Divergent cellular responses to CKS1i by healthy and malignant hematopoietic cells

To investigate the mechanism by which CKS1i induces divergent responses between healthy and malignant hematopoietic cells, we carried out proteomic analysis of *CKS1B*^{high} AML cell lines, which demonstrate direct correlation between *CKS1B* expression and CKS1i response, phenocopying primary patient AML (Fig. S7, Supp. Table S6), and umbilical cord blood derived healthy CD34$^+$ HSPCs, with and without CKS1i treatment in vitro (1μM; Figure 4A).

CKS1i treatment induced ~7.5x more differentially abundant proteins in THP-1 cells compared to healthy CD34$^+$ (Figure 4B-C). Differentially abundant cell cycle proteins demonstrated the divergent responses to CKS1i by healthy and malignant hematopoietic cells. Indeed, downregulation of cell cycle drivers and protein translation machinery in CD34$^+$ cells and upregulation of S phase promoting proteins in AML cells, with relatively few overlapping proteins (<10%), explains divergent cell cycle responses (Figure 4D-E).

Furthermore, key proteins differentially abundant in CD34$^+$ cells and not AML were integrated in three pathways fundamental to normal hematopoiesis: Wnt signalling, cell cycle control and NFκB signalling (Figure 4D, Fig. S8A). To investigate the changes in these key signalling pathways at single cell resolution we carried out mass cytometry with a panel of cell surface and intracellular markers covering signalling pathways important for HSPC proliferation, differentiation and stem cell self-renewal *(36)*.

Pseudo-bulk-level multidimensional scaling demonstrated a convergence of individual CD34$^+$ donors upon treatment with CKS1i (Fig. S8B). These differences in CD34$^+$ cells after CKS1i treatment were largely due to a reduction in abundance of intracellular signalling markers (Fig. S8C), particularly IκBα/NFκB signalling, CREB and mTOR phosphorylation (Figure 4F, Fig. S8D) and reduced proliferating cells (Figure 3C). Changes that were not observed in bulk AML or AML LSCs in response to CKS1i (Fig. S8E). In addition, the protein abundance of differentiation regulators such as PU.1 were also reduced (Fig. S8D), indicating a potential block in differentiation. Fewer cells had active non-phosphorylated β-catenin, demonstrating that the Wnt pathway – a fundamental pathway requiring a tight balance for normal hematopoiesis to proceed – was suppressed (Figure 4G, Fig. S8D).

Reduction of metabolically active markers like mTOR^{pS2448}, inflammatory responses including NFkB^{pS529}, and suppression of the translation machinery in our mass spectrometry analyses resulted in reduction of protein translation in CKS1i treated CD34^{+} cells (Figure 4H). Together, these signalling pathways are fundamental to the control of stress responses and particularly important to prevent the accumulation of lethal ROS in HSCs*(37)*. In agreement, CKS1i treatment reduced intracellular ROS in CD34^{+} cells (Figure 4I). CKS1i-dependent reduction of ROS surpassed that of NAC treatment, with no additive effects of CKS1i and NAC (Figure 4I). This led to improved stem cell frequency of CD34^{+} cells cultured in the presence of CKS1i (Fig. S8F).

The substantial changes in these key pathways are hallmarks of suppression of growth and differentiation, rather than an induction of cell death by CKS1i, confirming our functional data that HSC frequency increases when treated with CKS1i alone and CKS1i protects HSCs from the toxicity of Cytarabine/Doxorubicin (Figure 3I, Fig. S8F).

CKS1i induces an integrated molecular switch in AML cells driving RAC1 activity and NADP/H metabolism

Proteomic alterations mediated by CKS1i in AML revealed key changes beyond S phase accumulation, with modulators of the Ras-related C3 botulinum toxin substrate 1 (RAC1) and nicotinamide adenine dinucleotide phosphate (NADP/H) activity differentially abundant between control and CKS1i treated cells (Figure 5A, Fig. S9A-B).

Total RAC1 protein abundance was increased (Fig. S9C), as well as key interactors, such as Paxillin and CRK, after CKS1i treatment (Figure 5A). Mechanistically, inhibition of the SCF$^{SKP2\text{-}CKS1}$ complex led to accumulation of p27 (Fig. S9D), which inhibits RHOA activity (Figure 5B, Fig. S9E) *(38)*. This reduced the activity of RAC1-GTPase activating proteins (RAC-GAPs), to maintain RAC1 in its GTP bound state *(39)*, working in concert with RAC1 signalling pathway members to increase the amount of RAC1-GTP in AML after CKS1i treatment (Figure 5C, Fig. S9F).

RAC1-GTP together with NOXA(p67^{Phox}) regulates NADP to NADPH conversion – providing a pool for NADPH oxidases to produce ROS*(40)*. CKS1i altered a range of NADP/H metabolic regulators (Figure 5A). Thus, we evaluated the abundance and ratio of NADP/NADPH upon CKS1i treatment. CKS1i induced a dose dependent increase of NADPH in AML cells (Figure 5D-E, Fig. S10A-D). The accumulation of NADPH is dependent on RAC1-GTP activity, as CKS1i induction of NADPH was

rescued by the RAC1 inhibitor NSC23766 (NSC, Figure 5D-E. Fig. S10A-D). Sensitivity of the RHOA-RAC1 axis to CKS1i correlated with p27 stabilization (Fig. S9D) and IC_{50} values in *CKS1B*^{high} and *CKS1B*^{low} AML cell lines (Fig. S7), further demonstrating the dose-dependent sensitivity to CKS1i based on *CKS1B* expression. Together, these data demonstrate that inhibition of the $SCF^{SKP2\text{-}CKS1}$ complex induces an integrated molecular switch, with regulation of RAC1/NADPH activity maintained by convergent signalling pathways.

Inhibition of SCF-SKP2-CKS1 drives lethal ROS accumulation in AML

CKS1i-induced RAC1 activity and NADPH accumulation led to increased intracellular ROS in AML cell lines (Figure 5F-G, Fig. S10E-F), a phenotype conserved upon *CKS1B* knockdown (Figure 5H-J), indicating that CKS1 is critical to balance ROS abundance. Inhibition of RAC1 in cell lines rescued intracellular ROS accumulation induced by CKS1i or *CKS1B* knockdown (Figure 5F-J, Fig. S10E-F), and at higher doses was able to rescue CKS1i induced reduction in cell viability (Figure 5K-L, Fig. S10G-H).

Primary AML cells grown in vitro demonstrated similar sensitivity to CKS1i treatment, with induction of apoptosis in both bulk AML (Figure 5M) and importantly the LSC fraction of samples (Figure 5N). However, whereas RAC1 inhibition could improve the growth of AML, CKS1i effects on LSCs were dominant, maintaining LSC depletion during double treatment (Figure 5N, Fig S10I-K).

As the antioxidant N-acetyl-L-cysteine (NAC) is well known to scavenge intracellular ROS to reverse the negative effects of ROS on HSCs/LSCs, we tested whether NAC could reduce intracellular ROS accumulation and rescue survival. Indeed, NAC was able to reduce intracellular ROS in CKS1i treated AML cell lines (Figure 6A-C), and at higher doses NAC reversed CKS1i-dependent reduction in viability, demonstrating that CKS1i kills AML through accumulation of lethal ROS (Figure 6D-E). Additionally, increased intracellular ROS by CKS1i, or knockdown of *CKS1B,* led to induction of *CDKN1A* expression (Figure 6F-I), a known downstream effect of ROS causing cell cycle arrest and apoptosis.

Patient LSCs must maintain low ROS for survival*(41)*, and treatment of primary patient AML in vitro with CKS1i induced apoptosis in the LSC fraction and reduced both the proportion and total number of LSCs compared to control conditions (Figure 6J-L, Fig.

S10L-M). NAC treatment rescued CKS1i-induced LSC depletion in three out of four cases, returning LSC number similar to control conditions (Figure 6J-L).

These data demonstrate that AML requires $SCF^{SKP2\text{-}CKS1}$ functions to maintain a balance of intracellular ROS, which is critical for LSC maintenance in vivo. Ultimately, the increase in ROS, and the reduction in LSCs driven by CKS1i, indicates a clear pathway to target *CKS1B*^{high} LSCs in vivo*,* regardless of bulk *CKS1B* status in AML.

Combining CKS1 inhibition with induction chemotherapy simultaneously reduces LSCs, protects normal HSCs and improves overall survival

To test the potential for combining classical DA chemotherapy with CKS1i (DAC) in AML, we transplanted NSG mice with primary AML samples of varying *CKS1B* expression (Figure 7A). After stratifying for engraftment at week 4, we treated the mice with either DA or DAC. One-week post chemotherapy, xenografts showed strong reduction in leukemic burden in both DA and DAC treatment cohorts for all AMLs, regardless of *CKS1B* expression (Figure 7B). At the same time point, resident murine $CD45^+$ cells co-extracted from aspirated tibias had higher colony forming potential upon the addition of CKS1i compared to untreated mice and DA treated mice (Figure 7C), indicating that CKS1i treatment could selectively reduce AML, whilst simultaneously protecting normal HSPCs colony forming potential. Overall, DA treatment was only able to improve survival of one patient AML xenograft, due to the extensive by-toxicity of the treatment combined with AML burden in NSG mice. Addition of CKS1i improved overall survival of all patient AML xenografts, with many xenograft mice surviving up to 150 days (Figure 7D, Fig. S11A-D).

Examination of the normal hematopoietic compartment of xenografted mice at the end point of survival revealed a reduction in total number of long-term HSCs (LT-HSCs) in the DA treated group, whereas addition of CKS1i to DA abolished this effect, rescuing LT-HSC number (Figure 7E). In addition, the serial colony forming ability of normal murine HSPCs was improved in DAC conditions, indicating that rescued HSPCs were functional (Figure 7F).

We and others have documented the refractory nature of LSCs to induction chemotherapy*(42)*, and we set out to investigate the potential conflict or beneficial contribution between DA and CKS1i. In ex vivo conditions, both *CKS1B*$^{high\ \&\ low}$ AMLs (Figure 7G) showed a reduction in total cell number one week after DA or DAC treatment (Figure 7H), yet whilst DA treatment enriched for L-LTC-IC frequency in

three of the six patient samples, addition of CKS1i reduced L-LTC-IC frequency in all patients (Figure 7I & Fig S11E-F).

Finally, to investigate the reduction in LSC frequency conferred by CKS1i in vivo, we engrafted AML cells obtained from AML26 and AML32, which had the smallest improvement in overall survival after chemotherapy, in secondary recipient mice at limiting dilutions. Whilst control AMLs retained strong LSC frequency and showed robust engraftment after six weeks, frequency was increased by DA treatment in AML26 and was reduced in AML32 (Figure 7J-K, Fig. S12A-B). The addition of CKS1i counteracted the effect of DA by decreasing the LSC frequency in AML26 and further reducing LSC frequency in AML32 compared to DA and control mice, demonstrating strong reduction in LSCs after CKS1i treatment independent of the response to DA treatment (Figure 7J-K, Fig. S12A-B).

Overall secondary DA-AML mice survived longer than controls, and DAC-AML treated mice showed further improvement in survival, with no overt signs of sickness at 150 days in six of seven cases for both AML26 and AML32 (Figure 7L, Fig. S12C). Together, these data indicate that inhibition of CKS1-dependent protein degradation in combination with frontline chemotherapy is a more effective strategy to reduce the LSC pool, whilst protecting normal HSCs from chemotherapeutic toxicity.

Discussion

The difficulty of selectively targeting CSCs whilst simultaneously preserving normal stem cells is a major challenge in cancer therapy, and the study of normal and malignant hematopoietic stem cells has played a major role in understanding CSC biology*(43)*. In this study, we demonstrate that CKS1 is a key protein in this paradigm, with LSCs expressing higher CKS1 than most AML blasts, providing a selective vulnerability of LSCs to inhibition of the $SCF^{SKP2\text{-}CKS1}$ E3 ubiquitin ligase complex, while sparing normal HSCs from chemotherapeutic toxicity.

Poor risk AML is a heterogeneous group of cytogenetic abnormalities with very limited treatment options and extremely low overall survival rates*(1)*, even accounting for newer therapies, such as Venetoclax plus Azacitidine *(4, 5)*. While gene expression profiles, particularly those with single cell resolution, are improving our understanding of AML heterogeneity, the origins of relapse and revealing new clinical targets*(31)*, the role of proteostasis has been comparatively understudied*(44, 45)*. The selective

reduction of leukemic cells by CKS1 inhibition demonstrates that precisely targeting proteostatic regulators can be a new avenue in AML therapy.

Here we demonstrate that CKS1 regulates LSC viability through RAC1/NADPH/ROS pathways, fundamental in amplifying extrinsic and intrinsic signals in normal hematopoiesis and AML*(6, 46)*, and critical to metastatic disease across cancer*(47)*. The balance of intracellular ROS in normal and malignant hematopoietic stem cells has been of great interest in recent years*(37, 41)*, and changes in mitochondrial functions due to *RAS* mutations and nicotinamide-NAD metabolism underline the critical role for this pathway in primary patient resistance to Venetoclax*(6, 7)*. The induction of ROS in AML upon CKS1 inhibition demonstrates that the balance of CKS1-dependent protein degradation is key to maintaining stress responses in AML. This, together with LSCs requiring low ROS to maintain their stem cell potential, explains the strong reduction in LSC frequency conferred by CKS1i in primary patient AML (Figures 2 and 7).

The effect of CKS1i on normal hematopoiesis is clearly different to the effects observed in AML (Figure 3). Indeed, cell cycle blockage is highly beneficial, as patients treated with induction chemotherapy, which targets cycling cells, suffer from severe toxicity and cytopenia upon treatment. Classical induction chemotherapy is known to reduce the pool of hematopoietic progenitors, whilst quiescent HSCs are refractory to treatment, but ultimately undergo senescence*(48)*. It has previously been reported that deletion of *p27* in murine progenitors increased cycling and potency *(49)*. In agreement, we found that increased p27 protein and the accompanying cell cycle arrest of HSPCs by CKS1i could prevent DA reduction of normal cells in vivo (Figure 3), and in the context of AML could rescue the reduction in HSCs induced by chemotherapy (Figure 7). Importantly, CKS1i treatment also induced changes in fundamental HSPC signalling pathways involved in stem cell potency and response to stress. The overall suppression of key growth and activation cellular markers led to an opposite phenotype to that seen in AML cells, with a reduction in intracellular ROS and an increase in normal HSC frequency (Figure 4). In addition, CKS1i also rescues negative effects of induction chemotherapy on intestinal crypts (Fig. S6), a major issue associated with patient chemotherapeutic by-toxicity*(34, 35)*. Considering that older poor risk patients with AML patients (>65 years), who comprise the majority of AML cases, are ineligible for intensive chemotherapy *(50, 51)*, the reduction in toxicity

towards healthy tissue conferred by CKS1i during DA treatment has the potential to improve outcomes independent of direct AML effects.

The non-AML-intrinsic mechanism of action and effects on normal HSPCs by CKS1i may also implicate further components in the bone marrow niche. We and others have detailed the evolving bone marrow niche in hematological malignancies*(52)*, and the diverse repertoire of proteostatic machinery affected by CKS1i has the potential to affect cell competition in the leukemic bone marrow microenvironment by affecting normal HSPCs as well as stromal components.

Thus, the inhibition of CKS1-dependent protein degradation holds excellent promise for AML therapy, both as a single agent towards *CKS1B*^{high} AML, and in combination with induction chemotherapy in remaining AML cases. Reports of *CKS1B* overexpression correlating with outcome in other solid cancer types*(28, 30)*, and ways to modulate CKS1 activity*(53)*, indicate that proteostatic targeting, through this axis, holds much hope for future cancer therapy.

Limitations of study

The main limitation of our study is that we focus on a cohort of poor risk patients with AML which, despite covering a variety of cytogenetic and FAB subtypes, does not cover the full heterogeneity of patients with AML seen in the clinic. Further work will be needed to evaluate the efficacy of CKS1i on intermediate and good risk AML patient groups. As the combination of doxorubicin and cytarabine is quite toxic to the immunodeficient mice, it is not possible to combine this treatment with a preconditioning of the mice by sublethal irradiation. We were thus limited to testing combination approaches with patient AML samples capable of engrafting immunodeficient mice without prior conditioning. To mitigate this limitation, we tested a range of patient AML samples in ex vivo and in vitro conditions, to confirm all phenotypes through multiple assays.

Methods

Study design

This study aimed to investigate the sensitivity of poor risk AML to inhibition of CKS1-dependent protein degradation, as well as the potential side effect of this inhibitor on normal hematopoietic stem and progenitor cells. 32 primary poor risk AML patient

samples were obtained from St Bartholomew's Hospital as part of the poor risk AML consortium, of which 21 were suitable for drug screening and five were able to robustly engraft immunodeficient mouse models. We have performed several experiments using different approaches to address these objectives. We first analyzed whether the effect of CKS1i correlates to gene expression of *CKS1* in bulk AML samples. We also evaluated the protein expression of CKS1 in leukemic stem cells using mass cytometry analysis. We then evaluated the effect of CKS1i on primary poor risk AML and on normal hematopoietic stem/progenitor cells in vivo using immunodeficient mice. We also performed proteomic analysis on both normal and leukemic cells to investigate the mechanisms of action of CKS1i and used a RAC1 inhibitor (NSC23766) or N-Acetyl L Cysteine (NAC) to rescue the effects of CKS1i. Detailed below are all criteria for experimental cut-offs (e.g. mouse endpoint censure), number of cells used, blinding (all experiments were blinded during data collection unless otherwise stated) and statistical tests used.

Primary AML and UCB samples

AML samples were obtained after informed consent at St Bartholomew's Hospital (London, U.K.) at the time of diagnosis as part of the Bart's Cancer Institute Poor-Risk AML consortium. Full details of patient information are provided in Supplementary Table 1. Live mononuclear cells (MNCs) were isolated by density centrifugation using Ficoll-Paque (GE healthcare). Prior to culture or xenotransplantation, AML cells were depleted for T-cells using the Easysep T-cell depletion kit (StemCell Technologies). Umbilical Cord Blood (UCB) was obtained from full-term deliveries after informed consent, at the Royal London Hospital (London, U.K.). MNCs were isolated by density centrifugation using Ficoll-Paque (GE healthcare). Cells were selected for $CD34^+$ using the Easysep $CD34^+$ enrichment kit (StemCell Technologies). Purity was confirmed by flow cytometry. The collection and use of all human samples were approved by the East London Research Ethical Committee (REC:06/Q0604/110) and in accordance with the Declaration of Helsinki.

Patient derived xenografts (PDX) and in vivo drug treatment

All animal experiments were performed under the project license (PPL 70/8904) approved by the Home Office of the UK and in accordance with the Francis Crick institute animal ethics committee and ARRIVE guidelines. NOD-SCID IL2Rynull

(NSG) mice were originally a gift from Dr L. Schultz (Jackson Laboratory). These mice were rederived and bred since then at The Francis Crick Institute Biological Resources Facility.

Primary AML samples ($1x10^6$ – $5x10^6$ cells total) or UCB-$CD34^+$ ($5x10^4$ cells total) were injected intravenously (I.V.) into unconditioned 10-12 weeks old female or male NSG mice. After 4 weeks, engraftment was assessed by bone marrow aspiration from long bones whilst mice were under isoflurane anaesthesia. Mice were stratified according to engraftment and sex and assigned to treatment and control groups accordingly. Mice were treated as indicated with 10mg/kg CKS1i (Skp2-Cks1 E3 ligase inhibitor, Merck Millipore) intraperitoneal injection (I.P.) for 5 days, DA (doxorubicin/cytarabine, 1.5mg/kg/10mg/kg respectively, Sigma Aldrich), doxorubicin on days 1-3, cytarabine on days 1-5 co-injected I.V.*(33)*. Mice were scored for engraftment over the experimental course by bone marrow aspiration and for overall survival according to U.K. home office license protocols and following CRUK guidance (>20% peak body weight loss, overt signs of sickness/mortality).

Leukemic/Normal Long-term culture initiating cell (L-LTC-IC) assay

These experiments were performed as originally published by our group*(54)*. For all co-culture experiments, MS-5 stromal cells were seeded two days prior to AML/UCB cell addition at $4x10^5$ cells/ml to reach confluence at the time of irradiation. One day prior to AML/UCB addition, MS-5 stromal cells were irradiated with 7Gy and culture media was exchanged. On the day of starting co-culture, AML cells were plated at $2x10^5$ cells/ml in meylocult H5100 (StemCell Technologies) supplemented with IL-3, G-CSF and TPO (all 20ng/ml; Peprotech). UCB cells were plated at $2x10^5$ cells/ml in myelocult H5100 (StemCell Technologies). Half media changes were performed once per week without disrupting the feeder layer. At the start of week two, indicated drug treatments were added at 2x concentration in the half media change once. For L-LTC-CAFC assays, all cells were harvested at day 14 and sorted for live $hCD45^+mSca\text{-}1^-$ cells. Resulting cells were seeded in co-culture with fresh MS-5 stromal cells in a 96 well plate in a limiting dilution range (200,000 to 1,000) in 10 replicates and cultured for a further 5 weeks. At the end of the co-culture period cobblestone area forming cells were scored and L-LTC-IC frequency was calculated using the ELDA (Extreme Limiting Dilution Analysis) function in the Statmod R package.

For LTC-IC assays, media was continuous changed each week until week five, when cultures were harvested and live $hCD45^{+}mSca\text{-}1^{-}$ cells were sorted. Resulting cells were seeded in co-culture with fresh MS-5 stromal cells in a 96 well plate in a limiting dilution range (10,000 to 100) in 10 replicates and cultured for a further three weeks. At week eight, myelocult H5100 was replaced with Methocult methycellulose (StemCell Technologies H4434) for a further two weeks, after which wells were scored for colony-forming units and LTC-IC frequency was calculated using the ELDA (Extreme Limiting Dilution Analysis) function in the Statmod R package.

Protein translation assays

Protein translation was measured using the OP-Puromycin protein translation kit (Life Technologies). AML cell lines were seeded at $2x10^5$ cells/ml one day prior to treatment with the indicated drugs (day 0). The following day (day 1), drugs were added to culture wells at the indicated concentration. The next day (day 2), 10 μM OP-Puromycin was added to culture wells for one hour under culture conditions (37C, 5% CO_2). Cells were washed three times in ice-cold PBS and fixed in 4% paraformaldehyde (Sigma Aldrich) at room temperature for 15 mins in the dark. Cells were washed three times in PBS and permeabilised in PBS + 0.5% Triton X-100 (Sigma Aldrich) for 15 mins. Cells were washed twice in Click-IT reaction buffer wash solution and stained as per the manufacturer's instructions (Life Technologies). Abundance of OP-Puromycin was assessed using flow cytometry on a BD Fortessa FACS analyser.

Intracellular ROS staining

Intracellular reactive oxygen species were assayed using the CellRox deep red reagent (Life Technologies). AML cell lines were seeded at $2x10^5$ cells/ml one day prior to treatment with the indicated drugs (day 0). The following day (day 1), drugs were added to culture wells. The next day (day 2), CellRox deep red was added to each well at a final concentration of 5uM and verapamil was added at a final concentration of 50 μM. Cells were continued to be incubated in the same conditions (37C, 5% CO_2) for 1hr. After incubation, cells were collected from wells and washed three times in PBS + 1%FBS + 50 μM verapamil and finally resuspended in PBS + 1% FBS + 50 μM verapamil + DAPI (0.1μg/ml) before analysis on a BD Fortessa FACS analyser.

NADP/NADPH assays

Total NADP/H and NADPH were measured using the NADP/NADPH colorimetric assay kit (Abcam). AML cell lines were seeded at $2x10^5$ cells/ml one day prior to treatment with the indicated drugs (day 0). The following day (day 1), drugs were added to culture wells at the indicated concentration and cells were harvested after 8 hours. All cells were collected from the wells and washed three times in ice-cold PBS. Cells were lysed in NADP/NADPH extraction buffer by performing two freeze/thaw cycles (20 mins on dry ice followed by 10 mins at room temperature). Lysates were centrifuged at 13,000g for 10minutes and the supernatant was retained. Lysate supernatant was split in half, with one half remaining on ice and the other half incubated at 60C for 30mins to remove $NADP^+$. Total NADP/H (NADPt) and NADPH only lysates were run in 96 well plates with freshly made standards as per the manufacturers' instructions. NADP/NADPH ratio was calculated as (NADPt-NADPH)/NADPH.

Mass Cytometry

CyTOF preparation and analysis was carried out as per our previous publication *(36)*. Cultured cells were washed in ice-cold PBS three times and incubated with 5μM Cisplatin (Fluidigm) to mark dead cells. Cells were washed three times in ice-cold PBS and fixed in 1.6% formaldehyde (Sigma Aldrich). Fixed cells were surface stained with the relevant antibodies (resources table) for two hours at room temperature followed by three washes with PBS. Cells were permeabilised in 1ml Perm buffer III (BD biosciences) on ice for 30mins, washed three times in ice-cold PBS and incubated with the relevant intracellular antibodies (resources table) overnight at 4ºC with gentle rotation. Resulting cells were wash three times in ice-cold PBS and stained with 100nM Iridium in PBS + 0.1% Saponin (Riedel-de Haen) overnight before analysis on a Helios Mass Cytometer (Fluidigm). All control and CKS1i treated samples were prepared simultaneously with equal buffers, antibodies and fixation.

Publicly available datasets

CKS1B expression in normal and malignant hematopoiesis was obtained through Bloodspot.eu. Overall survival and stratification for *CKS1B* expression was calculated from data obtained from The Cancer Genome Atlas (TCGA). AML cell line RNA

sequencing data was obtained from the EBI Expression Atlas (RNA-seq of 934 Human cancer cell lines from the Cancer Cell Line Encyclopedia).

Statistics and data interpretation

Results shown are +/-SEM unless otherwise indicated. To compare treatment versus control in all in vitro and in vivo experiments, a Student's *t*-test was used as indicated in the figure legend with N number indicated. For all comparisons, unpaired *t*-tests were undertaken unless otherwise indicated. All repeat samples presented are from biological replicates of distinct samples/xenotransplantations. Survival analyses were carried out using the "survminer" package on R to calculate significance between Kaplan-Meier curves and Hazard ratios. Kaplan Meier graphs were plotted using Graphpad Prism. Correlation analyses were carried out using the "performance analytics" and "corrplot" packages in R. Multiple DSS comparisons with *CKS1B* expression were carried out with pairwise complete observations using Spearman, Pearson and Kendall correlation coefficients. Individual correlations for *CKS1B* vs DSS or IC_{50} were plotted using Graphpad Prism. Stem cell frequency was calculated using the extreme limiting dilution analysis (ELDA) function in the "statmod" R package*(55)*. Pathway analysis and enrichment was run through MetaCore (genego.com) and network interactions produced on String (string-db.org). CyTOF analysis was conducted using the CATALYST package on gated live, single cells.

Acknowledgements

We would like to acknowledge the Francis Crick core flow cytometry, cell services and biological research facility STPs. We would like to acknowledge Drs R. Hynds, H Wood, D. Taussig & Prof. P. Parker for their critical feedback on the manuscript. Graphical abstract was created with BioRender.com.

Funding

This works was supported partly by Cancer Research UK (FC001115 to DB), the UK Medical Research Council (FC001115 to DB), the Wellcome Trust (FC001115 to DB), a CRUK program grant (C15966/A24375 to JF & DB) and Leukaemia U.K. (2021/JGF/002 to WG). For the purpose of Open Access, the authors have applied a

CC BY public copyright license to any Author Accepted Manuscript version arising from this submission.

Author contributions

W.G. Conceived the study, designed and carried out experiments, analyzed data and wrote the manuscript. A.R-M. Analyzed patient data. P.C-I. Carried out mass spectrometry analyses. E.G. carried out experiments and analyzed data. J.J.M. Designed and carried out experiments. S.A. Analyzed data. F.B-C. Analyzed data. A.P. Designed and carried out experiments. C.A.H. Undertook drug screening. P.C. Undertook mass spectrometry analyses. C.S. Provided LGR5 mice and gut preparations. J.G. Provided patient samples and data. J.F. Provided patient samples and data. D.B. Conceived the study and wrote the manuscript. All authors provided critical feedback on the manuscript pre-submission.

Competing interests

C.S. acknowledges grant support from AstraZeneca, Boehringer-Ingelheim, Bristol Myers Squibb, Pfizer, Roche-Ventana, Invitae (previously Archer Dx Inc - collaboration in minimal residual disease sequencing technologies), and Ono Pharmaceutical. He is an AstraZeneca Advisory Board member and Chief Investigator for the AZ MeRmaiD 1 and 2 clinical trials and is also chief investigator of the NHS Galleri trial. He has consulted for Achilles Therapeutics, Amgen, AstraZeneca, Pfizer, Novartis, GlaxoSmithKline, MSD, Bristol Myers Squibb, Illumina, Genentech, Roche-Ventana, GRAIL, Medicxi, Metabomed, Bicycle Therapeutics, Roche Innovation Centre Shanghai, and the Sarah Cannon Research Institute. C.S. had stock options in Apogen Biotechnologies and GRAIL until June 2021, and currently has stock options in Epic Bioscience, Bicycle Therapeutics, and has stock options and is co-founder of Achilles Therapeutics. P.C. is co-founder and director of Kinomica Ltd.

Patents: C.S. holds patents relating to assay technology to detect tumour recurrence (PCT/GB2017/053289); to targeting neoantigens (PCT/EP2016/059401), identifying patient response to immune checkpoint blockade (PCT/EP2016/071471), determining HLA LOH (PCT/GB2018/052004), predicting survival rates of patients with cancer (PCT/GB2020/050221), identifying patients who respond to cancer treatment (PCT/GB2018/051912), US patent relating to detecting tumour mutations (PCT/US2017/28013), methods for lung cancer detection (US20190106751A1) and

both a European and US patent related to identifying insertion/deletion mutation targets (PCT/GB2018/051892).

Data and materials availability

All data associated with this study are present in the paper or supplementary materials. The mass spectrometry proteomics data have been deposited to the ProteomeXchange Consortium via the PRIDE partner repository (PXD022754 and 10.6019/PXD022754).

Supplementary Materials

Supplementary materials and methods

Supplementary

Fig. S1. To S12.

Supplementary table S1. To S7.

References

1. H. Döhner, D. J. Weisdorf, C. D. Bloomfield, D. L. Longo, Ed. Acute Myeloid Leukemia, *N. Engl. J. Med.* **373**, 1136–1152 (2015).

2. L. I. Shlush, A. Mitchell, L. Heisler, S. Abelson, S. W. K. Ng, A. Trotman-Grant, J. J. F. Medeiros, A. Rao-Bhatia, I. Jaciw-Zurakowsky, R. Marke, J. L. McLeod, M. Doedens, G. Bader, V. Voisin, C. Xu, J. D. McPherson, T. J. Hudson, J. C. Y. Wang, M. D. Minden, J. E. Dick, Tracing the origins of relapse in acute myeloid leukaemia to stem cells, *Nature* (2017), doi:10.1038/nature22993.

3. T. C. Ho, M. LaMere, B. M. Stevens, J. M. Ashton, J. R. Myers, K. M. O'Dwyer, J. L. Liesveld, J. H. Mendler, M. Guzman, J. D. Morrissette, J. Zhao, E. S. Wang, M. Wetzler, C. T. Jordan, M. W. Becker, Evolution of acute myelogenous leukemia stem cell properties after treatment and progression, *Blood* (2016), doi:10.1182/blood-2016-02-695312.

4. C. D. DiNardo, I. S. Tiong, A. Quaglieri, S. MacRaild, S. Loghavi, F. C. Brown, R. Thijssen, G. Pomilio, A. Ivey, J. M. Salmon, C. Glytsou, S. A. Fleming, Q. Zhang, H.

709 Ma, K. P. Patel, S. M. Kornblau, Z. Xu, C. C. Chua, X. Chen, P. Blombery, C.
710 Flensburg, N. Cummings, I. Aifantis, H. Kantarjian, D. C. S. Huang, A. W. Roberts, I.
711 J. Majewski, M. Konopleva, A. H. Wei, Molecular patterns of response and treatment
712 failure after frontline venetoclax combinations in older patients with AML, *Blood* **135**,
713 791–803 (2020).
714 5. C. D. DiNardo, B. A. Jonas, V. Pullarkat, M. J. Thirman, J. S. Garcia, A. H. Wei, M.
715 Konopleva, H. Döhner, A. Letai, P. Fenaux, E. Koller, V. Havelange, B. Leber, J.
716 Esteve, J. Wang, V. Pejsa, R. Hájek, K. Porkka, Á. Illés, D. Lavie, R. M. Lemoli, K.
717 Yamamoto, S.-S. Yoon, J.-H. Jang, S.-P. Yeh, M. Turgut, W.-J. Hong, Y. Zhou, J.
718 Potluri, K. W. Pratz, Azacitidine and Venetoclax in Previously Untreated Acute
719 Myeloid Leukemia, *N. Engl. J. Med.* **383**, 617–629 (2020).
720 6. C. L. Jones, B. M. Stevens, D. A. Pollyea, R. Culp-Hill, J. A. Reisz, T. Nemkov, S.
721 Gehrke, F. Gamboni, A. Krug, A. Winters, S. Pei, A. Gustafson, H. Ye, A. Inguva, M.
722 Amaya, M. Minhajuddin, D. Abbott, M. W. Becker, J. DeGregori, C. A. Smith, A.
723 D'Alessandro, C. T. Jordan, Nicotinamide Metabolism Mediates Resistance to
724 Venetoclax in Relapsed Acute Myeloid Leukemia Stem Cells, *Cell Stem Cell* (2020),
725 doi:10.1016/j.stem.2020.07.021.
726 7. B. M. Stevens, C. L. Jones, D. A. Pollyea, R. Culp-Hill, A. D'Alessandro, A.
727 Winters, A. Krug, D. Abbott, M. Goosman, S. Pei, H. Ye, A. E. Gillen, M. W. Becker,
728 M. R. Savona, C. Smith, C. T. Jordan, Fatty acid metabolism underlies venetoclax
729 resistance in acute myeloid leukemia stem cells, *Nat. Cancer* , 1–12 (2020).
730 8. W. Grey, A. Ivey, T. A. Milne, T. Haferlach, D. Grimwade, F. Uhlmann, E. Voisset,
731 V. Yu, The Cks1/Cks2 axis fine-tunes Mll1 expression and is crucial for MLL-
732 rearranged leukaemia cell viability, *Biochim. Biophys. Acta - Mol. Cell Res.* **1865**,
733 105–116 (2018).
734 9. R. C. Rao, Y. Dou, Hijacked in cancer: The KMT2 (MLL) family of
735 methyltransferases*Nat. Rev. Cancer* **15**, 334–346 (2015).
736 10. J. Grinat, J. Heuberger, R. O. Vidal, N. Goveas, F. Kosel, A. Berenguer-Llergo,
737 A. Kranz, A. Wulf-Goldenberg, D. Behrens, B. Melcher, S. Sauer, M. Vieth, E. Batlle,
738 A. F. Stewart, W. Birchmeier, The epigenetic regulator Mll1 is required for Wnt-driven
739 intestinal tumorigenesis and cancer stemness, *Nat. Commun.* (2020),
740 doi:10.1038/s41467-020-20222-z.
741 11. M. Frontini, A. Kukalev, E. Leo, Y.-M. M. Ng, M. Cervantes, C.-W. W. Cheng, R.
742 Holic, D. Dormann, E. Tse, Y. Pommier, V. P. C. C. Yu, The CDK Subunit CKS2

743 Counteracts CKS1 to Control Cyclin A/CDK2 Activity in Maintaining Replicative
744 Fidelity and Neurodevelopment, *Dev. Cell* **23**, 356–370 (2012).
745 12. R. Wolthuis, L. Clay-Farrace, W. van Zon, M. Yekezare, L. Koop, J. Ogink, R.
746 Medema, J. Pines, Cdc20 and Cks direct the spindle checkpoint-independent
747 destruction of cyclin A, *Mol Cell* **30**, 290–302 (2008).
748 13. H. S. Martinsson-Ahlzen, V. Liberal, B. Grunenfelder, S. R. Chaves, C. H.
749 Spruck, S. I. Reed, H.-S. Martinsson-Ahlzén, V. Liberal, B. Grünenfelder, S. R.
750 Chaves, C. H. Spruck, S. I. Reed, Cyclin-dependent kinase-associated proteins
751 Cks1 and Cks2 are essential during early embryogenesis and for cell cycle
752 progression in somatic cells, *Mol Cell Biol* **28**, 5698–5709 (2008).
753 14. M. C. Morris, P. Kaiser, S. Rudyak, C. Baskerville, M. H. Watson, S. I. Reed,
754 Cks1-dependent proteasome recruitment and activation of CDC20 transcription in
755 budding yeast., *Nature* **423**, 1009–1013 (2003).
756 15. S. V Del Rincón, M. Widschwendter, D. Sun, S. Ekholm-Reed, J. Tat, L. K.
757 Teixeira, Z. Ellederova, E. Grolieres, S. I. Reed, C. Spruck, Cks overexpression
758 enhances chemotherapeutic efficacy by overriding DNA damage checkpoints.,
759 *Oncogene* , 1–7 (2014).
760 16. V. Liberal, H.-S. Martinsson-Ahlzén, J. Liberal, C. H. Spruck, M. Widschwendter,
761 C. H. McGowan, S. I. Reed, H. S. Martinsson-Ahlzen, J. Liberal, C. H. Spruck, M.
762 Widschwendter, C. H. McGowan, S. I. Reed, Cyclin-dependent kinase subunit (Cks)
763 1 or Cks2 overexpression overrides the DNA damage response barrier triggered by
764 activated oncoproteins., *Proc. Natl. Acad. Sci. U. S. A.* **109**, 2754–9 (2012).
765 17. C. Spruck, H. Strohmaier, M. Watson, A. P. L. Smith, A. Ryan, W. Krek, S. I.
766 Reed, A CDK-independent function of mammalian Cks1: Targeting of SCFSkp2 to
767 the CDK inhibitor p27Kip1, *Mol. Cell* **7**, 639–650 (2001).
768 18. A. Mocciaro, M. Rape, Emerging regulatory mechanisms in ubiquitindependent
769 cell cycle control*J. Cell Sci.* **125** (2012), doi:10.1242/jcs.091199.
770 19. A. Daulny, W. P. Tansey, Damage control: DNA repair, transcription, and the
771 ubiquitin-proteasome system*DNA Repair (Amst).* **8** (2009),
772 doi:10.1016/j.dnarep.2009.01.017.
773 20. A. V. Sorokin, A. A. Selyutina, M. A. Skabkin, S. G. Guryanov, I. V. Nazimov, C.
774 Richard, J. Th'Ng, J. Yau, P. H. B. Sorensen, L. P. Ovchinnikov, V. Evdokimova,
775 Proteasome-mediated cleavage of the Y-box-binding protein 1 is linked to DNA-
776 damage stress response, *EMBO J.* **24** (2005), doi:10.1038/sj.emboj.7600830.

21. X. Zhang, S. Linder, M. Bazzaro, Drug development targeting the ubiquitin-proteasome system (UPS) for the treatment of human cancers*Cancers (Basel).* **12** (2020), doi:10.3390/cancers12040902.
22. R. Aplenc, S. Meshinchi, L. Sung, T. Alonzo, J. Choi, B. Fisher, R. Gerbing, B. Hirsch, T. Horton, S. Kahwash, J. Levine, M. Loken, L. Brodersen, J. Pollard, S. Raimondi, E. A. Kolb, A. Gamis, Bortezomib with standard chemotherapy for children with acute myeloid leukemia does not improve treatment outcomes: a report from the Children's Oncology Group, *Haematologica* **105** (2020), doi:10.3324/haematol.2019.220962.
23. R. T. Swords, S. Coutre, M. B. Maris, J. F. Zeidner, J. M. Foran, J. Cruz, H. P. Erba, J. G. Berdeja, W. Tam, S. Vardhanabhuti, I. Pawlikowska-Dobler, H. M. Faessel, A. B. Dash, F. Sedarati, B. J. Dezube, D. V. Faller, M. R. Savona, Pevonedistat, a first-in-class NEDD8-activating enzyme (NAE) inhibitor, combined with azacitidine, in patients with AML, *Blood* **228**, blood-2017-09-805895 (2018).
24. L. Zhou, S. Chen, Y. Zhang, M. Kmieciak, Y. Leng, L. Li, H. Lin, K. A. Rizzo, C. I. Dumur, A. Ferreira-Gonzalez, M. Rahmani, L. Povirk, S. Chalasani, A. J. Berger, Y. Dai, S. Grant, The NAE inhibitor pevonedistat interacts with the HDAC inhibitor belinostat to target AML cells by disrupting the DDR., *Blood* **127**, 2219–30 (2016).
25. J. F. Zeidner, F. Mazerolle, J. A. Bell, L. E. Cain, D. V. Faller, M. Dalal, A. Regnault, R. J. Fram, Randomized Phase 2 Trial of Pevonedistat Plus Azacitidine Versus Azacitidine in Higher-Risk Myelodysplastic Syndromes/Chronic Myelomonocytic Leukemia or Low-Blast Acute Myeloid Leukemia: Exploratory Analysis of Patient-Reported Outcomes, *Blood* **136** (2020), doi:10.1182/blood-2020-136935.
26. L. Wu, A. V Grigoryan, Y. Li, B. Hao, M. Pagano, T. J. Cardozo, Specific small molecule inhibitors of Skp2-mediated p27 degradation., *Chem. Biol.* **19**, 1515–24 (2012).
27. S. C. Pavlides, K.-T. Huang, D. A. Reid, L. Wu, S. V Blank, K. Mittal, L. Guo, E. Rothenberg, B. Rueda, T. Cardozo, L. I. Gold, Inhibitors of SCF-Skp2/Cks1 E3 ligase block estrogen-induced growth stimulation and degradation of nuclear p27kip1: therapeutic potential for endometrial cancer., *Endocrinology* **154**, 4030–45 (2013).
28. D.-Y. Y. Shen, Z.-X. X. Fang, P. You, P.-G. G. Liu, F. Wang, C.-L. L. Huang, X.-B. B. Yao, Z.-X. X. Chen, Z.-Y. Y. Zhang, Clinical significance and expression of

cyclin kinase subunits 1 and 2 in hepatocellular carcinoma, *Liver Int* **30**, 119–125 (2010).
29. S. Kitajima, Y. Kudo, I. Ogawa, T. Bashir, M. Kitagawa, M. Miyauchi, M. Pagano, T. Takata, Role of Cks1 overexpression in oral squamous cell carcinomas: cooperation with Skp2 in promoting p27 degradation., *Am. J. Pathol.* **165**, 2147–2155 (2004).
30. T.-A. Masuda, H. Inoue, K. Nishida, H. Sonoda, Y. Yoshikawa, Y. Kakeji, T. Utsunomiya, M. Mori, Cyclin-dependent kinase 1 gene expression is associated with poor prognosis in gastric carcinoma., *Clin. Cancer Res.* **9**, 5693–5698 (2003).
31. P. Van Galen, V. Hovestadt, M. H. W. Ii, J. C. Aster, A. A. Lane, B. E. Bernstein, P. Van Galen, V. Hovestadt, M. H. W. Ii, T. K. Hughes, G. K. Griffin, S. Battaglia, J. A. Verga, J. Stephansky, T. J. Pastika, J. L. Story, Single-Cell RNA-Seq Reveals AML Hierarchies Relevant to Disease Progression and Immunity Article Single-Cell RNA-Seq Reveals AML Hierarchies Relevant to Disease Progression and Immunity, *Cell* (2019).
32. B. de Boer, J. Prick, M. G. Pruis, P. Keane, M. R. Imperato, J. Jaques, A. Z. Brouwers-Vos, S. M. Hogeling, C. M. Woolthuis, M. T. Nijk, A. Diepstra, S. Wandinger, M. Versele, R. M. Attar, P. N. Cockerill, G. Huls, E. Vellenga, A. B. Mulder, C. Bonifer, J. J. Schuringa, Prospective Isolation and Characterization of Genetically and Functionally Distinct AML Subclones, *Cancer Cell* **34**, 674-689.e8 (2018).
33. M. Wunderlich, B. Mizukawa, F. S. Chou, C. Sexton, M. Shrestha, Y. Saunthararajah, J. C. Mulloy, AML cells are differentially sensitive to chemotherapy treatment in a human xenograft model, *Blood* (2013), doi:10.1182/blood-2012-10-464677.
34. A. Camera, C. Andretta, M. R. Villa, M. Volpicelli, M. Picardi, M. Rossi, C. R. Rinaldi, P. Della Cioppa, R. Ciancia, C. Selleri, B. Rotoli, Intestinal toxicity during induction chemotherapy with cytarabine-based regimens in adult acute myeloid leukemia, *Hematol. J.* (2003), doi:10.1038/sj.thj.6200304.
35. E. J. Bow, J. B. Meddings, Intestinal mucosal dysfunction and infection during remission-induction therapy for acute myeloid leukaemia, *Leukemia* (2006), doi:10.1038/sj.leu.2404440.
36. W. Grey, R. Chauhan, M. Piganeau, H. Huerga Encabo, M. Garcia-Albornoz, N. Q. McDonald, D. Bonnet, Activation of the receptor tyrosine kinase, RET, improves

long-term hematopoietic stem cell outgrowth and potency, *Blood* (2020), doi:10.1182/blood.2020006302.
37. A. Ludin, S. Gur-Cohen, K. Golan, K. B. Kaufmann, T. Itkin, C. Medaglia, X. J. Lu, G. Ledergor, O. Kollet, T. Lapidot, Reactive oxygen species regulate hematopoietic stem cell self-renewal, migration and development, as well as their bone marrow microenvironment*Antioxidants Redox Signal.* (2014), doi:10.1089/ars.2014.5941.
38. A. Kukalev, Y.-M. Ng, L. Ju, A. Saidi, S. Lane, A. Mondragon, D. Dormann, S. E. Walker, W. Grey, P. W.-L. Ho, D. N. Stephens, A. M. Carr, K. Lamsa, E. Tse, V. P. C. C. Yu, Deficiency of Cks1 Leads to Learning and Long-Term Memory Defects and p27 Dependent Formation of Neuronal Cofilin Aggregates., *Cereb. Cortex* **27**, 11–23 (2017).
39. L. K. Nguyen, B. N. Kholodenko, A. von Kriegsheim, Rac1 and RhoA: Networks, loops and bistability*Small GTPases* **9** (2018), doi:10.1080/21541248.2016.1224399.
40. F. Jiang, G. S. Liu, G. J. Dusting, E. C. Chan, NADPH oxidase-dependent redox signaling in TGF-β-mediated fibrotic responses*Redox Biol.* (2014), doi:10.1016/j.redox.2014.01.012.
41. E. D. Lagadinou, A. Sach, K. Callahan, R. M. Rossi, S. J. Neering, M. Minhajuddin, J. M. Ashton, S. Pei, V. Grose, K. M. O'Dwyer, J. L. Liesveld, P. S. Brookes, M. W. Becker, C. T. Jordan, BCL-2 inhibition targets oxidative phosphorylation and selectively eradicates quiescent human leukemia stem cells, *Cell Stem Cell* (2013), doi:10.1016/j.stem.2012.12.013.
42. A. Di Tullio, K. Rouault-Pierre, A. Abarrategi, S. Mian, W. Grey, J. Gribben, A. Stewart, E. Blackwood, D. Bonnet, The combination of CHK1 inhibitor with G-CSF overrides cytarabine resistance in human acute myeloid leukemia, *Nat. Commun.* **8**, 1679 (2017).
43. E. Batlle, H. Clevers, Cancer stem cells revisited*Nat. Med.* (2017), doi:10.1038/nm.4409.
44. S. Raffel, D. Klimmeck, M. Falcone, A. Demir, A. Pouya, P. Zeisberger, C. Lutz, M. Tinelli, O. Bischel, L. Bullinger, C. Thiede, A. Flörcken, J. Westermann, G. Ehninger, A. D. Ho, C. Müller-Tidow, Z. Gu, C. Herrmann, J. Krijgsveld, A. Trumpp, J. Hansson, Quantitative proteomics reveals specific metabolic features of Acute Myeloid Leukemia stem cells, *Blood* (2020), doi:10.1182/blood.2019003654.
45. E. Aasebø, A. Brenner, F. Berven, Ø. Bruserud, F. Selheim, M. Hernandez-

879 Valladares, Proteomic Profiling of Primary Human Acute Myeloid Leukemia Cells
880 Does Not Reflect Their Constitutive Release of Soluble Mediators, *Proteomes* **7**, 1
881 (2018).
882 46. J. C. Mulloy, J. A. Cancelas, M. D. Filippi, T. A. Kalfa, F. Guo, Y. Zheng, Rho
883 GTPases in hematopoiesis and hemopathies*Blood* (2010), doi:10.1182/blood-2009-
884 09-198127.
885 47. M. del M. Maldonado, J. I. Medina, L. Velazquez, S. Dharmawardhane, Targeting
886 Rac and Cdc42 GEFs in Metastatic Cancer*Front. Cell Dev. Biol.* (2020),
887 doi:10.3389/fcell.2020.00201.
888 48. L. Shao, Y. Wang, J. Chang, Y. Luo, A. Meng, D. Zhou, Hematopoietic stem cell
889 senescence and cancer therapy-induced long-term bone marrow injury, *Transl.*
890 *Cancer Res.* (2013), doi:10.3978/j.issn.2218-676X.2013.10.05.
891 49. T. Cheng, N. Rodrigues, D. Dombkowski, S. Stier, D. T. Scadden, Stem cell
892 repopulation efficiency but not pool size is governed by p27(kip1)., *Nat. Med.* **6**,
893 1235–1240 (2000).
894 50. H. Kantarjian, S. O'Brisn, J. Cortes, F. Giles, S. Faderl, E. Jabbour, G. Garcia-
895 Manero, W. Wierda, S. Pierce, J. Shan, E. Estey, Results of intensive chemotherapy
896 in 998 patients age 65 years or older with acute myeloid leukemia or high-risk
897 myelodysplastic syndrome: Predictive prognostic models for outcome, *Cancer*
898 (2006), doi:10.1002/cncr.21723.
899 51. H. Kantarjian, F. Ravandi, S. O'Brien, J. Cortes, S. Faderl, G. Garcia-Manero, E.
900 Jabbour, W. Wierda, T. Kadia, S. Pierce, J. Shan, M. Keating, E. J. Freireich,
901 Intensive chemotherapy does not benefit most older patients (age 70 years or older)
902 with acute myeloid leukemia, *Blood* (2010), doi:10.1182/blood-2010-03-276485.
903 52. A. Batsivari, W. Grey, D. Bonnet, Understanding of the crosstalk between normal
904 residual hematopoietic stem cells and the leukemic niche in acute myeloid leukemia,
905 *Exp. Hematol.* (2021), doi:10.1016/j.exphem.2021.01.004.
906 53. A. Hamdi, A. Lesnard, P. Suzanne, T. Robert, M. a Miteva, M. Pellerano, B.
907 Didier, E. Ficko-Blean, A. Lobstein, M. Hibert, S. Rault, M. C. Morris, P. Colas,
908 Tampering with cell division by using small-molecule inhibitors of CDK-CKS protein
909 interactions., *Chembiochem* **16**, 432–9 (2015).
910 54. E. Griessinger, F. Anjos-Afonso, I. Pizzitola, K. Rouault-Pierre, J. Vargaftig, D.
911 Taussig, J. Gribben, F. Lassailly, D. Bonnet, A niche-like culture system allowing the
912 maintenance of primary human acute myeloid leukemia-initiating cells: a new tool to

913 decipher their chemoresistance and self-renewal mechanisms., *Stem Cells Transl.*
914 *Med.* **3**, 520–9 (2014).
915

Figure Legends

Figure 1. Inhibition of CKS1-dependent protein degradation kills AML blast. A. Expression of *CKS1B* (relative to *GAPDH*) in a poor risk AML cohort. FAB and p53 status are indicated for each patient (FAB color coded, p53 status: white = WT; black = mutant; *n*=32). **B.** Diagram of action for CKS1i binding and inhibition of the $SCF^{SKP2\text{-}CKS1}$ ubiquitin ligase complex. **C.** Correlation between CKS1i drug sensitivity (DSS) and *CKS1B* expression (relative to *GAPDH*) **D.** Percentage of human $CD45^+$ cells of total $CD45^+$ cells in mouse bone marrow aspirations one week after chemotherapy (week 6). **E.** Correlation between *CKS1B* expression and reduction in human AML burden post CKS1i treatment. **F-J.** Kaplan Meier plots and *P* value calculated (Mantel-Cox test) for each individual PDX control and CKS1i treated cohort. Each data point represents one mouse. A Student's *t*-test was used to calculate significance of difference for all graphs unless otherwise stated. * $P<0.05$; ** $P<0.005$.

Figure 2. AML LSCs have high CKS1 expression and are sensitive to CKS1i. A. *t*-stochastic neighbor embedding of patient AML7 illustrating co-expression of CKS1 protein with key LSC cell surface markers. **B.** Median intensity of CKS1 protein abundance in bulk AML versus LSCs. **C.** Individual 1/L-LTC-IC frequencies with upper and lower limits for each patient tested. Control (Grey) vs CKS1i (Blue). **D.** Fold change L-LTC-IC frequency, CKS1i treatment versus control for all patient samples tested. **E.** Overall survival of AML26 secondary transplantation with the indicated cell doses from primary treatment mice. **F.** Estimated LSC frequency of secondary transplanted AML26. Control calculated at week 6, CKS1i calculated at the end point of the experiment. **G.** Percentage of apoptotic (Annexin V positive) LSCs in control and CKS1i treated primary patient AML in vitro 24 hours after treatment. **H.** Percentage of LSCs in total AML cells in control and CKS1i treated primary patient AML in vitro 24 hours after treatment. A Student's *t*-test was used to calculate significance of difference for all graphs unless otherwise stated. * $P<0.05$; ** $P<0.005$; *** $P< 0.0005$.

Figure 3. CKS1i protects normal hematopoietic cells from chemotherapeutic toxicity by suppressing the cell cycle. A. Percentage Annexin V positive apoptotic cells for the indicated cell types in response to increasing concentrations of CKS1i. **B.** p27 protein mean fluorescent intensity measured in $CD34^+$ cells cultured with CKS1i (1μM) in the indicated cell populations. **C.** Cell cycle profile and **D.** Total cell count of $CD34^+$ cells treated with the indicated doses of CKS1i (1μM for live cell count) for 24 hours. **E.** Illustration of $CD34^+$ engraftment and chemotherapeutic treatment in NSG mice. **F.** Change in percentage human $CD45^+$ of total CD45 at the indicated time points for Control (Ctrl), Doxorubicin/Cytarabine (DA) and Doxorubicin/Cytarabine plus CKS1i (DAC) treatments. **G.** Fold change of the percentage of human CD45 cells at week 4 and 6 for the indicated treatments (Control = Grey, DA = Green, DAC = Blue). **H.** Representative flow plots and **I.** Percentage of total cells annexin V positive after 6 weeks in vivo for human CD45 cells with the indicated treatment conditions (Ctrl N=5, DA N=3, DAC N=3). **J.** HSC frequency calculated by limiting dilution secondary transplantation of human $CD45^+$ cells retrieved from primary mice (Control = Grey, DA = Green, DAC = Blue). A Student's *t*-test was used to calculate significance of difference unless otherwise stated. * $P<0.05$; ** $P<0.005$.

Figure 4. CKS1i treatment induces divergent proteomic alterations in normal and malignant hematopoietic cells. A. Workflow for timescale of cell preparation for mass spectrometry analysis. Volcano plots for proteomic alterations in **B.** THP-1 and **C.** $CD34^+$ cells in response to CKS1i (1μM). **D.** Key differentially abundant proteins in THP-1 or $CD34^+$ cells in response to CKS1i (*n*=4 per condition). **E.** Venn diagram depicting overlap of differentially expressed proteins between THP-1 and $CD34^+$ cells. **F.** Median expression of key intracellular signalling markers identified in CyTOF analyses after CKS1i treatment (Ctrl *n*=3, CKS1i *n*=4). **G.** Representative flow plots and quantified mean fluorescence intensity for non-phosphorylated β-catenin in $CD34^+$ cells grown for 48 hours in control conditions or treated with CKS1i (*n*=4). **H.** Representative flow plots (including cells grown without OP-Puromycin; -OPP) and % total OP-Puromycin incorporation in $CD34^+$ cells grown for 48 hours in control conditions or treated with CKS1i. OP-Puromycin was added 1hr prior to collection and fixation of cells (*n*=4). **I.** Representative flow plots and quantified mean fluorescence intensity of intracellular reactive oxygen species (ROS) in $CD34^+$ cells grown for 48

hours in control conditions or treated with CKS1i (1μM) or NAC (1.25mM; *n*=3 per condition). * *P*<0.05; ***P*<0.005; ****P*<0.0005; *****P*<0.0001.

Figure 5. The $SCF^{SKP2\text{-}CKS1}$ complex controls RAC1/NADPH/ROS signalling. A. String network analysis of key differentially abundant proteins in THP-1 cells treated with CKS1i. Red indicates upregulated, and blue indicates downregulated in response to CKS1i treatment. **B.** RHOA-GTP and **C.** RAC1-GTP abundance in THP-1 cells control or treated with CKS1i (1 μM) for 24 hours (*n*=3 independent experiments). Total NADPH (pmol) in **D.** THP-1 and **E.** HL60 cells treated with the indicated doses of CKS1i (+ = 1μM, ++ = 5μM) or NSC23766 (NSC; + = 0.1μM, ++ = 1μM) for 8 hours (*n*=4 independent experiments per cell line and treatment). **F.** Representative flow plots and **G.** Quantified mean fluorescence intensity of intracellular reactive oxygen species (ROS) in the indicated cell lines in response to CKS1i (+ = 1μM) and NSC (+ = 0.1μM) treatment (*n*=3 per cell line and treatment). **H.** Representative flow plots and **I-J.** Quantified mean fluorescence intensity of intracellular reactive oxygen species (ROS) in the indicated cell lines in response to *CKS1B* knockdown and NSC (+ = 0.1μM) treatment (*n*=3 per cell line and treatment). **K-L.** Viability represented by percentage reduction O_2 of the indicated cell lines in response to the indicated concentrations of CKS1i and NSC23766 (*n*=5 per cell line and treatment, except THP-1 where *n*=6), CKS1i (+ = 1μM) and NSC (+ = 0.1μM, ++ = 1μM). **M.** Percentage Annexin V positive apoptotic primary patient AML samples treated with the indicated doses of CKS1i (+ = 1μM) and NSC (+ = 0.1μM). **N.** Fold change cell number versus control for total AML (Blasts) and LSCs with the indicated treatments (CKS1i + = 1μM and NSC + = 0.1μM) 24 hours after treatment in vitro. A Student's *t*-test was used to calculate significance of difference for all graphs. * *P*<0.05; ***P*<0.005; *** *P*< 0.0005; **** *P*< 0.0001.

Figure 6. CKS1i treatment depletes LSCs by inducing lethal ROS. A. Representative flow plots and **B-C.** Quantified mean fluorescence intensity (MFI) of intracellular reactive oxygen species (ROS) in the indicated cell lines in response to CKS1i (+ = 1μM, ++ = 5μM) and NAC (+ = 1.25mM, ++ = 2.5mM) treatment (N=3 per cell line and treatment). **D-E.** Viability represented by percentage reduction O_2 of the indicated cell lines in response to the indicated concentrations of CKS1i (+ = 1μM, ++ = 5μM) and NAC (+ = 1.25mM, ++ = 2.5mM; N=3 per cell line). Quantitative PCR analysis of *CDKN1A* expression in **F.** THP-1 cells treated with CKS1i, **G.** THP-1 cells with *CKS1B* knockdown, **H.** HL-60 cells treated with CKS1i and **I.** HL60 cells with *CKS1B* knockdown for 24 hours (*n*=3). **J.** Induction of apoptosis (Annexin V+) in primary patient LSCs in response to CKS1i and NAC (CKS1i + = 1μM, NAC + = 1.25mM) 24 hours after treatment in vitro. **K.** Percentage LSCs of total primary patient AML blasts in response to CKS1i and NAC (CKS1i + = 1μM, NAC + = 1.25mM) 24 hours after treatment in vitro. **L.** Fold change absolute number of primary patient LSCs in the indicated treatments versus control (CKS1i + = 1μM, CKS1i ++ = 5μM, NAC + = 1.25mM, NAC ++ = 2.5mM) 24 hours after treatment in vitro. A Student's *t*-test was used to calculate significance of difference for all graphs. * $P<0.05$; ** $P<0.005$; *** $P<0.0005$; **** $P<0.0001$.

Figure 7. Combination of induction chemotherapy and CKS1i reduces AML burden and LSC potential whilst protecting resident hematopoietic cells. A. *CKS1B* expression (relative to *GAPDH*) for patient AMLs tested in vivo. **B.** Percentage of human $CD45^+$ cells of total $CD45^+$ cells in mouse bone marrow aspirations one week after chemotherapy (week 6). **C.** Colony forming units per 10,000 mouse $CD45^+$ cells extracted from week 6 bone marrow aspirations. **D.** Swimmer plots and *P* values calculated (Mantel-Cox test) for each individual PDX Control and treated mouse cohort. Each data point represents one mouse and days survived are presented. Treatment interval is illustrated as annotated. **E.** Total number of murine Long-term HSCs obtained from bone marrow of mice at the final survival time point (Ctrl *n*=8, DA *n*=5, DAC *n*=5). **F.** Serial colony forming units per 10,000 mouse $CD45^+$ cells obtained from BM of mice at the final survival time point (Ctrl *n*=6, DA *n*=5, DAC *n*=6). **G.** *CKS1B* expression (relative to *GAPDH*) for patient AMLs tested in L-LTC-IC. **H.** Fold change of live human $CD45^+$ cells, indicated treatments versus control, after two weeks of co-culture. **I.** Fold change of L-LTC-IC frequency of indicated treatment versus control, after 7 weeks of co-culture. **J-K.** LSC frequency in secondary transplanted mice injected with AML26 or AML32 at limiting dilutions 6 weeks post-transplantation. **L.** Kaplan-Meier survival curve for AML32 secondary mice up to 120 days. A Student's *t*-test was used to calculate significance of difference for all graphs unless otherwise stated. * $p<0.05$; ** $p<0.005$; *** $p< 0.0005$.

Figure 1.

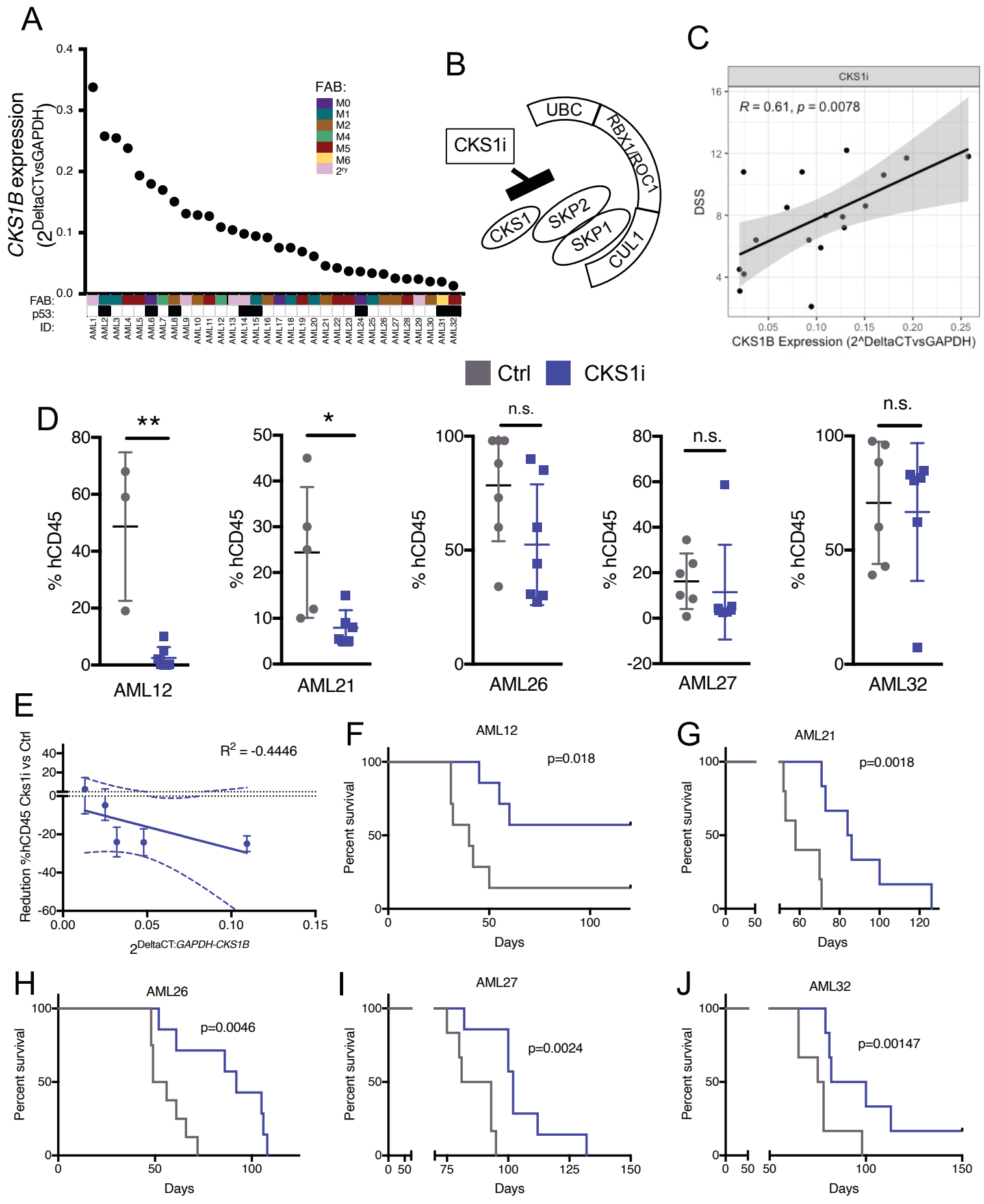
A
CKS1B expression (2DeltaCTvsGAPDH)
FAB:
M0
M1
M2
M4
M5
M6
2ry
p53:
ID:
B
UBC
RBX1/ROC1
CKS1i
CKS1
SKP2
SKP1
CUL1
C
CKS1i
R = 0.61, p = 0.0078
DSS
CKS1B Expression (2^DeltaCTvsGAPDH)
Ctrl
CKS1i
D
% hCD45
**
*
n.s.
n.s.
n.s.
AML12
AML21
AML26
AML27
AML32
E
Redution %hCD45 Cks1i vs Ctrl
R2 = -0.4446
2DeltaCT:GAPDH-CKS1B
F
AML12
p=0.018
Percent survival
Days
G
AML21
p=0.0018
Percent survival
Days
H
AML26
p=0.0046
Percent survival
Days
I
AML27
p=0.0024
Percent survival
Days
J
AML32
p=0.00147
Percent survival
Days

Figure 2.

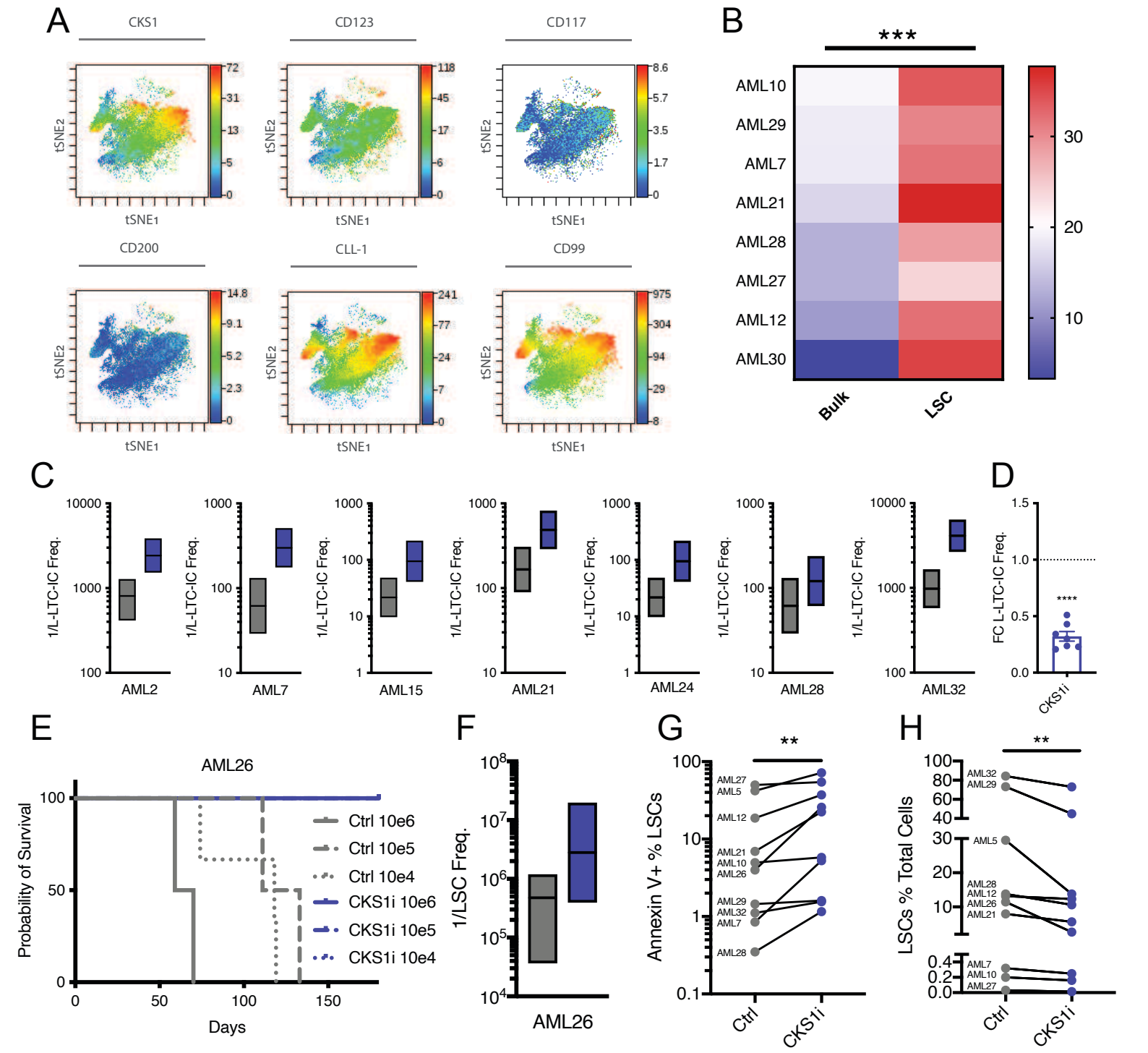
A
CKS1
CD123
CD117
CD200
CLL-1
CD99
tSNE1
tSNE2
B
***
AML10
AML29
AML7
AML21
AML28
AML27
AML12
AML30
Bulk
LSC
C
1/L-LTC-IC Freq.
AML2
AML7
AML15
AML21
AML24
AML28
AML32
D
FC L-LTC-IC Freq.
****
CKS1i
E
AML26
Probability of Survival
Days
Ctrl 10e6
Ctrl 10e5
Ctrl 10e4
CKS1i 10e6
CKS1i 10e5
CKS1i 10e4
F
1/LSC Freq.
AML26
G
**
Annexin V+ % LSCs
Ctrl
CKS1i
H
**
LSCs % Total Cells
Ctrl
CKS1i

Figure 3.

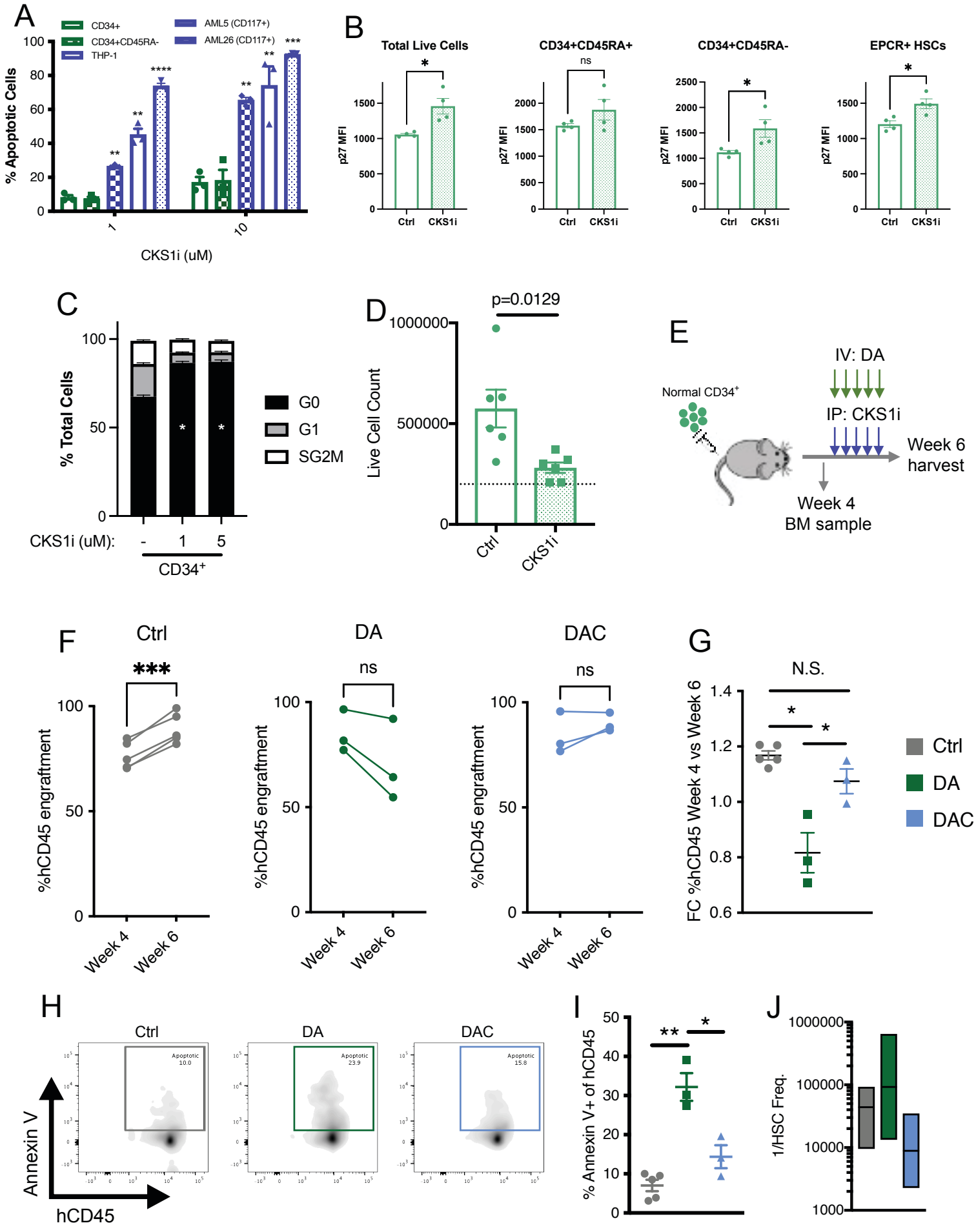
A
CD34+
CD34+CD45RA-
THP-1
AML5 (CD117+)
AML26 (CD117+)
% Apoptotic Cells
CKS1i (uM)
B
Total Live Cells
CD34+CD45RA+
CD34+CD45RA-
EPCR+ HSCs
p27 MFI
Ctrl
CKS1i
ns
C
% Total Cells
G0
G1
SG2M
CKS1i (uM):
CD34+
D
p=0.0129
Live Cell Count
E
Normal CD34+
IV: DA
IP: CKS1i
Week 6 harvest
Week 4 BM sample
F
Ctrl
DA
DAC
%hCD45 engraftment
Week 4
Week 6
G
N.S.
FC %hCD45 Week 4 vs Week 6
H
Annexin V
hCD45
Apoptotic
I
% Annexin V+ of hCD45
J
1/HSC Freq.

Figure 4.

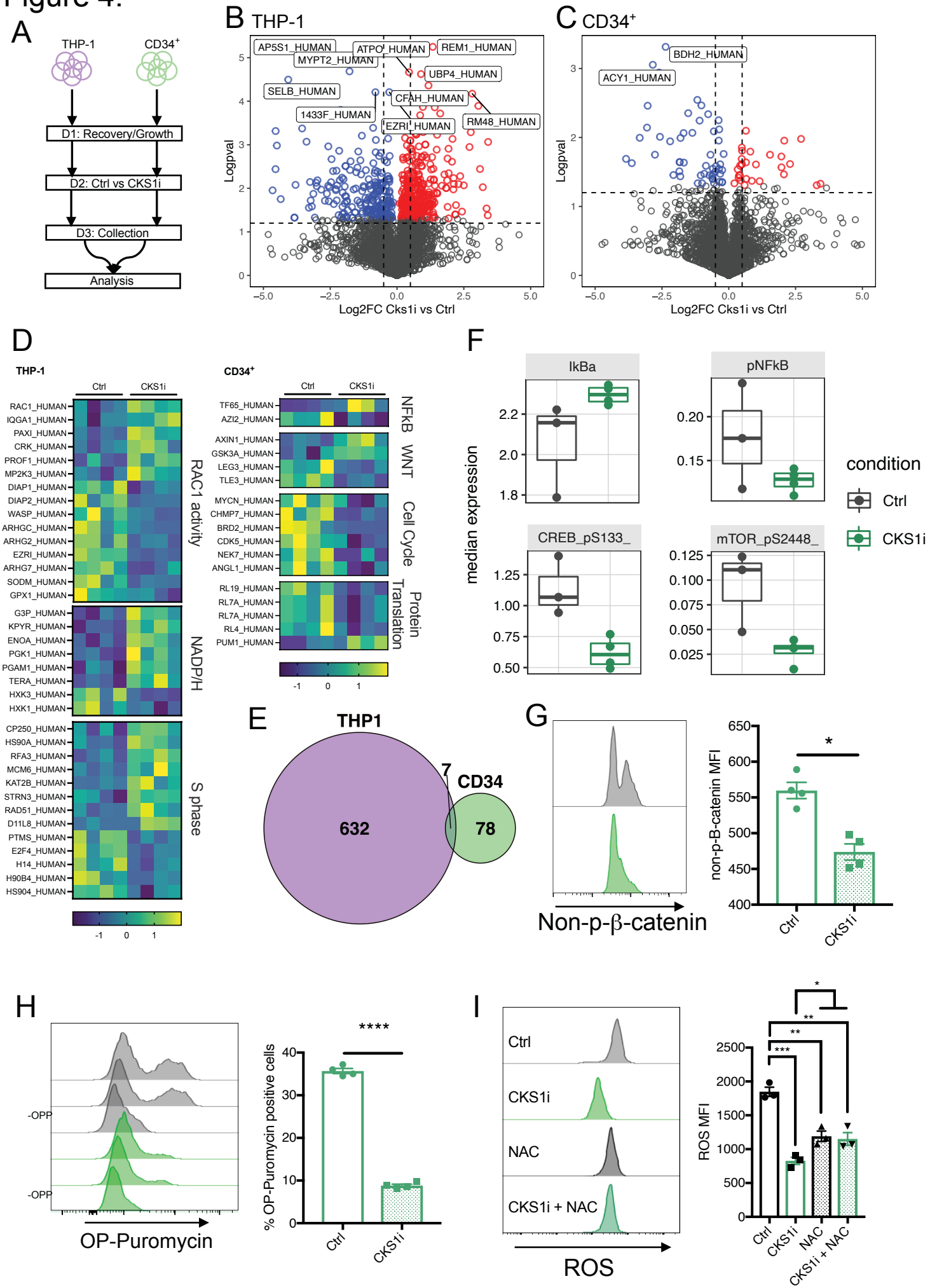
A
THP-1
CD34+
D1: Recovery/Growth
D2: Ctrl vs CKS1i
D3: Collection
Analysis
B THP-1
AP5S1_HUMAN
MYPT2_HUMAN
ATPO_HUMAN
REM1_HUMAN
UBP4_HUMAN
SELB_HUMAN
CFAH_HUMAN
1433F_HUMAN
EZRI_HUMAN
RM48_HUMAN
Logpval
Log2FC Cks1i vs Ctrl
C CD34+
BDH2_HUMAN
ACY1_HUMAN
Logpval
Log2FC Cks1i vs Ctrl
D
THP-1
CD34+
Ctrl
CKS1i
RAC1_HUMAN
IQGA1_HUMAN
PAXI_HUMAN
CRK_HUMAN
PROF1_HUMAN
MP2K3_HUMAN
DIAP1_HUMAN
DIAP2_HUMAN
WASP_HUMAN
ARHGC_HUMAN
ARHG2_HUMAN
EZRI_HUMAN
ARHG7_HUMAN
SODM_HUMAN
GPX1_HUMAN
RAC1 activity
G3P_HUMAN
KPYR_HUMAN
ENOA_HUMAN
PGK1_HUMAN
PGAM1_HUMAN
TERA_HUMAN
HXK3_HUMAN
HXK1_HUMAN
NADP/H
CP250_HUMAN
HS90A_HUMAN
RFA3_HUMAN
MCM6_HUMAN
KAT2B_HUMAN
STRN3_HUMAN
RAD51_HUMAN
D11L8_HUMAN
PTMS_HUMAN
E2F4_HUMAN
H14_HUMAN
H90B4_HUMAN
HS904_HUMAN
S phase
TF65_HUMAN
AZI2_HUMAN
NFkB
AXIN1_HUMAN
GSK3A_HUMAN
LEG3_HUMAN
TLE3_HUMAN
WNT
MYCN_HUMAN
CHMP7_HUMAN
BRD2_HUMAN
CDK5_HUMAN
NEK7_HUMAN
ANGL1_HUMAN
Cell Cycle
RL19_HUMAN
RL7A_HUMAN
RL7A_HUMAN
RL4_HUMAN
PUM1_HUMAN
Protein Translation
F
IkBa
pNFkB
CREB_pS133_
mTOR_pS2448_
median expression
condition
Ctrl
CKS1i
E
THP1
CD34
632
7
78
G
Non-p-β-catenin
non-p-B-catenin MFI
Ctrl
CKS1i
H
-OPP
-OPP
OP-Puromycin
% OP-Puromycin positive cells
****
Ctrl
CKS1i
I
Ctrl
CKS1i
NAC
CKS1i + NAC
ROS
ROS MFI
Ctrl
CKS1i
NAC
CKS1i + NAC

Figure 5.

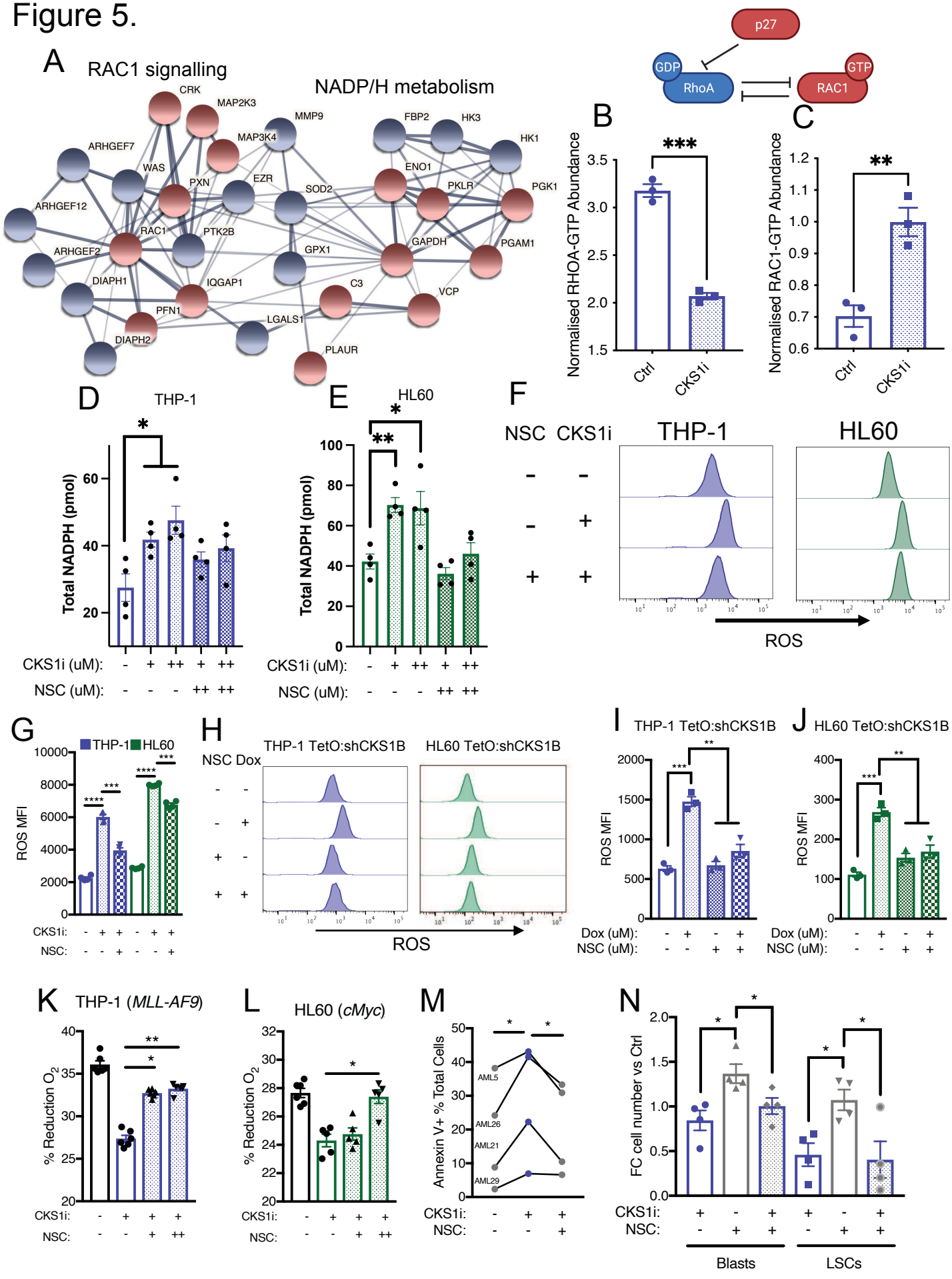
A
RAC1 signalling
NADP/H metabolism
CRK
MAP2K3
MMP9
MAP3K4
ARHGEF7
WAS
PXN
EZR
SOD2
ARHGEF12
RAC1
PTK2B
ARHGEF2
GPX1
DIAPH1
IQGAP1
C3
VCP
PFN1
LGALS1
DIAPH2
PLAUR
FBP2
HK3
HK1
ENO1
PKLR
PGK1
GAPDH
PGAM1
p27
GDP
RhoA
GTP
RAC1
B
Normalised RHOA-GTP Abundance
***
Ctrl
CKS1i
C
Normalised RAC1-GTP Abundance
**
Ctrl
CKS1i
D
THP-1
Total NADPH (pmol)
CKS1i (uM):
NSC (uM):
E
HL60
Total NADPH (pmol)
CKS1i (uM):
NSC (uM):
F
NSC CKS1i
THP-1
HL60
ROS
G
THP-1 HL60
ROS MFI
CKS1i:
NSC:
H
NSC Dox
THP-1 TetO:shCKS1B
HL60 TetO:shCKS1B
ROS
I
THP-1 TetO:shCKS1B
ROS MFI
Dox (uM):
NSC (uM):
J
HL60 TetO:shCKS1B
ROS MFI
Dox (uM):
NSC (uM):
K
THP-1 (MLL-AF9)
% Reduction O2
CKS1i:
NSC:
L
HL60 (cMyc)
% Reduction O2
CKS1i:
NSC:
M
Annexin V+ % Total Cells
AML5
AML26
AML21
AML29
CKS1i:
NSC:
N
FC cell number vs Ctrl
CKS1i:
NSC:
Blasts
LSCs

Figure 6.

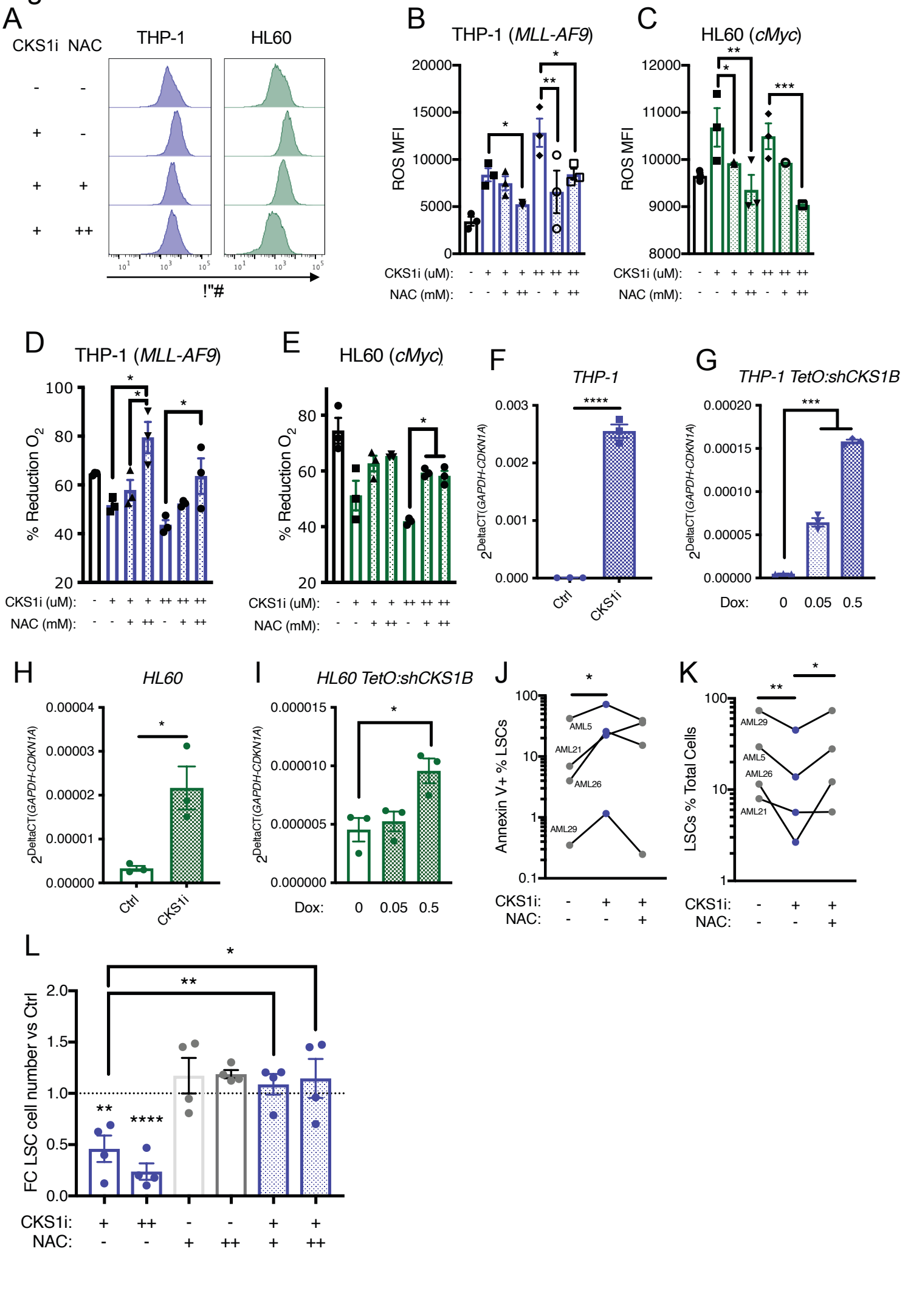
A
CKS1i NAC
THP-1
HL60
B
THP-1 (MLL-AF9)
ROS MFI
C
HL60 (cMyc)
ROS MFI
CKS1i (uM):
NAC (mM):
D
THP-1 (MLL-AF9)
% Reduction O2
E
HL60 (cMyc)
% Reduction O2
F
THP-1
2DeltaCT(GAPDH-CDKN1A)
Ctrl
CKS1i
G
THP-1 TetO:shCKS1B
2DeltaCT(GAPDH-CDKN1A)
Dox:
H
HL60
2DeltaCT(GAPDH-CDKN1A)
I
HL60 TetO:shCKS1B
2DeltaCT(GAPDH-CDKN1A)
J
Annexin V+ % LSCs
AML5
AML21
AML26
AML29
K
LSCs % Total Cells
L
FC LSC cell number vs Ctrl

Figure 7.

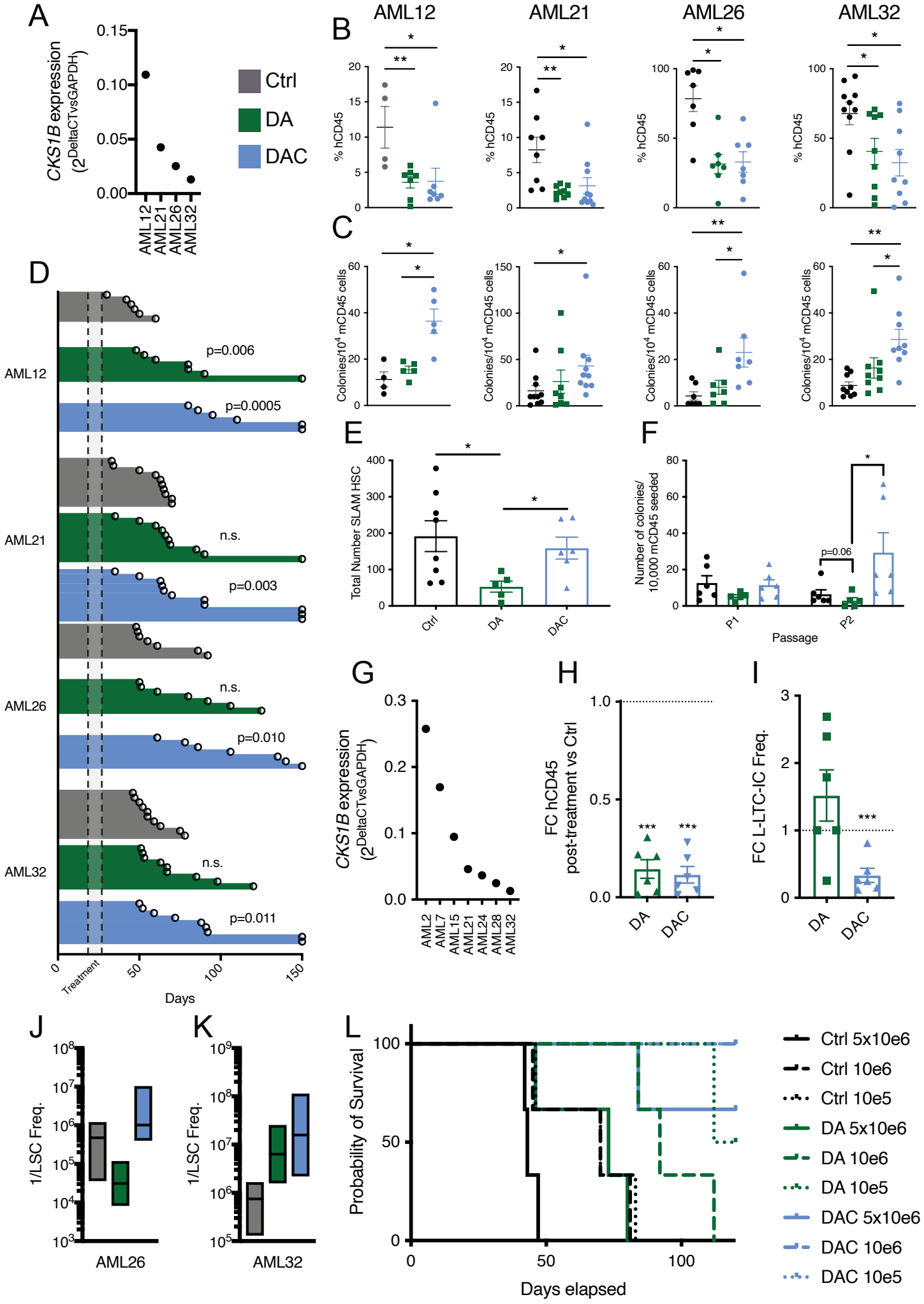
A
CKS1B expression (2DeltaCTvsGAPDH)
Ctrl
DA
DAC
AML12
AML21
AML26
AML32
B
C
% hCD45
Colonies/10^4 mCD45 cells
D
p=0.006
p=0.0005
n.s.
p=0.003
n.s.
p=0.010
n.s.
p=0.011
Treatment
Days
E
Total Number SLAM HSC
F
Number of colonies/ 10,000 mCD45 seeded
p=0.06
P1
P2
Passage
G
AML2
AML7
AML15
AML21
AML24
AML28
AML32
H
FC hCD45 post-treatment vs Ctrl
I
FC L-LTC-IC Freq.
J
1/LSC Freq.
K
L
Probability of Survival
Days elapsed
Ctrl 5x10e6
Ctrl 10e6
Ctrl 10e5
DA 5x10e6
DA 10e6
DA 10e5
DAC 5x10e6
DAC 10e6
DAC 10e5

Supplementary Information

Supplementary Methods

AML cell line, AML primary sample, UCB CD34$^+$ and MS-5 culture

All AML cell lines and MS-5 stromal cells were originally obtained from the ATCC and maintained by the Francis Crick Cell Services. Before using these lines, they were authenticated using the Short Tandem Repeat (SRF) profiling and tested for mycoplasma prior to commencing experiments. All AML cell lines were cultured in RPMI 1640, 10% heat-inactivated FBS and 1% penicillin/streptomycin (Life Technologies) at 37ºC, 5% CO_2. Umbilical cord blood CD34$^+$ cells were cultured in StemSpan SFEMMII (StemCell Technologies) supplemented with Human SCF (150ng/ml), Human FLT3 ligand (150ng/ml) and Human TPO (20ng/ml; all Peprotech) at 2x10^5 cells/ml at 37ºC, 5% CO_2. For relative viability, apoptosis and IC_{50} calculations cell lines were seeded in 96 well plates at a concentration of 2x10^5 cells/ml with the indicated dose of drug. Measurements of viability (% reduction O_2) or apoptosis (Annexin V positivity) were taken at 48 hours post-treatment. MS-5 stromal cells were cultured in IMDM, 10% heat-inactivated FBS and 2% penicillin/streptomycin (Life Technologies) at 37ºC, 5% CO_2. Primary human AML samples were recovered for 24 hours in StemSpan SFEMMII (Stem Cell Technologies) supplemented with IL-3, G-CSF, TPO (20ng/ml each; all Peprotech) and treated as indicated.

Mass Spectrometry

THP-1 AML cell lines and UCB CD34$^+$ cells were cultured as per culture and drug treatment in methods. Cells were recovered for 24 hours in their respective media followed by sub-lethal AML doses of CKS1i (1μM) for 12 hours. All cells were retrieved from wells, washed three times in ice-cold PBS and snap frozen in liquid nitrogen as dry pellets. Cells were cultured in the conditions above, with differing media compositions.

Cell pellets were lysed in 100 μL of urea buffer (8 M urea in 20 mM HEPES, pH: 8.0), lysates were further homogenized by sonication (30 cycles of 30s on 30s off; Diagenode Bioruptor Plus) and insoluble material was removed by centrifugation. Protein amount was quantified using BCA (Thermo Fisher Scientific). Then, 100 and 20 μg of protein for THP-1 and CD34$^+$ samples, respectively, were diluted in urea

buffer to a final volume of 300 μL and subjected to cysteine alkylation using sequential incubation with 10 mM dithiothreitol (DDT) and 16.6 mM iodoacetamide (IAM) for 1 h and 30 min, respectively, at 25 °C with agitation. Trypsin beads (50% slurry of TLCK-trypsin; Thermo-Fisher Scientific; Cat. #20230) were equilibrated with 3 washes with 20 mM HEPES (pH 8.0), the urea concentration in the protein suspensions was reduced to 2 M by the addition of 900 μL of 20 mM HEPES (pH 8.0), 100 μL of equilibrated trypsin beads were added and samples were incubated overnight at 37°C. Trypsin beads were removed by centrifugation (2000 xg at 5°C for 5 min) and the resulting peptide solutions were desalted using carbon C18 spin tips (Glygen; Cat. # TT2MC18). Briefly, spin tips were activated twice with 200 μL of Elution Solution (70% ACN, 0.1% TFA) and equilibrated twice with 200 μL of Wash Solution (1% ACN, 0.1% TFA). Samples were loaded and spin tips were washed twice with 200 μL of Wash Solution. Peptides were eluted into fresh tubes from the spin tips with 4 times with 50 μl of Elution Solution. In each of the desalting steps, spin tips were centrifuged at 1,500xg at 5C for 3 min. Finally, samples were dried in a SpeedVac and peptide pellets were stored at −80°C.

For mass spectrometry identification and quantification of proteins, samples were run twice in a LC-MS/MS platform. Briefly, peptide pellets were resuspended in 100 μL and 20 μL of reconstitution buffer (20 fmol/μL enolase in 3% ACN, 0.1% TFA) for THP-1 and $CD34^+$ samples, respectively. Then, 2 μL were loaded onto an LC-MS/MS system consisting of a Dionex UltiMate 3000 RSLC coupled to a Q Exactive Plus Orbitrap Mass Spectrometer (Thermo Fisher Scientific) through an EASY-Spray source (Cat. # ES081, Thermo Fisher Scientific). Mobile phases for the chromatographic separation of the peptides consisted in Solvent A (3% ACN: 0.1% FA) and Solvent B (99.9% ACN; 0.1% FA). Peptides were loaded in a micro-pre-column (Acclaim PepMap 100 C18 LC; Cat. # 160454, Thermo Fisher Scientific) and separated in an analytical column (Acclaim PepMap 100 C18 LC; Cat. # 164569, Thermo Fisher Scientific) using a gradient running from 3% to 23% over 120 min. The UPLC system delivered a flow of 2 μL/min (loading) and 300 nL/min (gradient elution). The Q-Exactive Plus operated a duty cycle of 2.1s. Thus, it acquired full scan survey spectra (m/z 375–1500) with a 70,000 FWHM resolution followed by data-dependent acquisition in which the 15 most intense ions were selected for HCD (higher energy collisional dissociation) and MS/MS scanning (200–2000 m/z) with a resolution of

17,500 FWHM. A dynamic exclusion period of 30s was enabled with a m/z window of ±10 ppms.

Peptide identification from MS data was automated using a Mascot Daemon 2.5.0 workflow in which Mascot Distiller v2.5.1.0 generated peak list files (MGFs) from RAW data and the Mascot search engine (v2.5) matched the MS/MS data stored in the MGF files to peptides using the SwissProt Database (SwissProt_2016Oct.fasta). Searches had a FDR of ~1% and allowed 2 trypsin missed cleavages, mass tolerance of ±10 ppm for the MS scans and ±25 mmu for the MS/MS scans, carbamidomethyl Cys as a fixed modification and PyroGlu on N-terminal Gln and oxidation of Met as variable modifications. Identified peptides were quantified using Pescal software in a label free procedure based on extracted ion chromatograms (XICs). Thus, the software constructed XICs for all the peptides identified across all samples with mass and retention time windows of ±7 ppm and ±2 min, respectively and calculated the area under the peak. Individual peptide intensity values in each sample were normalized to the sum of the intensity values of all the peptides quantified in that sample. Data points not quantified were given a peptide intensity value equal to the minimum intensity value quantified in the sample divided by 10. Protein intensity values were calculated by adding the individual normalized intensities of all the peptides comprised in a protein and values of 2 technical replicates per sample were averaged. Protein score values were expressed as the maximum Mascot protein score value obtained across samples.

Drug sensitivity and resistance testing (DSRT)

Single drug DSRT was performed as described previously*(52)*. In brief, compounds, each with 7 different concentrations, were pre-plated using an acoustic liquid handling Echo 550 (Labcyte) to 384-well plates. Primary AML cells were suspended in conditioned medium (RPMI 1640 supplemented with 10% fetal bovine serum, 2mM L-glutamine, penicillin-100U/ml, streptomucing-100ug/ml and 12.5% conditioned medium from HS-5 human bone marrow stromal cells), DNase I treated for 4h (Promega), filtered through a 70μm cell strainer (Thermo Fisher Scientific) to remove possible cell clumps, and viable cells were counted. Pre-plated compounds in each 384-well plate were dissolved in 5ul of conditioned medium using a MultiDrop Combi peristaltic dispenser (Thermo Fisher Scientific) and shaken for 5 minutes to dissolve

the compounds. AML cells were plated at 5,000 cells/well in 20ul, leading to a final volume of 25ul/well. Plates were gently shaken for 5 minutes to mix the cells with the compounds and incubated for 72 hours at 37ºC, 5% CO_2.

Cell viability was measured using the CellTiter-Glo assay (Promega) with a PHERAstar microplate reader (BMG-labtech). Data was normalised to negative (DMSO only) and positive control wells (100uM benzethonium chloride) and dose response curves calculated.

Ex vivo drug sensitivity of AML cells to the tested drugs was calculated using a drug sensitivity score (DSS), a modified form of the area under the inhibition curve calculation that integrates multiple dose response parameters for each of the tested drugs, as previously described*(53)*.

Intestinal crypt analyses

Tamoxifen (Sigma, #T5648) was dissolved in ethanol to 300 mg/ml and further diluted in sunflower seed oil (Sigma #S5007) to a final concentration of 30 mg/ml. To induce recombination, 6-14 weeks old $Lgr5^{tm1(cre/ERT2)Cle}$ mice were given one dose of tamoxifen (150 ug/g body weight) via oral gavage. After 24h, chemotherapy was administered as described above. After seven days the animals were culled, the intestines harvested and fixed in 10% neutral buffered formalin for 24h and subsequently transferred to 70% ethanol. After embedding and sectioning, the slides were stained with anti-EGFP (LGR5) or Ki67 and the number of positive crypts (LGR5) or cells per crypt (Ki67) were counted.

AML cell line in vivo experimentation

AML cell lines were transduced with GFP-Luciferase containing vectors as per our previous reports *(41)*. For both cell lines (THP-1 and HL60) $2x10^6$ cells were injected I.V. into unconditioned 10-12 weeks old female or male NSG mice. After 7 days engraftment was assessed by bioluminescence imaging. Isofluorane anesthetized mice were imaged 5-10 minutes post D-luciferin injection I.P. (15mg.kg; Caliper life sciences) using the Xenogen IVIS imaging system. Photons emitted were expressed as Flux (photons/s/cm^2), and quantified and analysed using “living image” software (Caliper life sciences).

Colony forming units

For resident mouse hematopoietic cell response to 5-FU', CKS1i, DA and DAC, colony forming ability was assessed in methylcellulose (StemCell Technologies M3434-GF). 10^4 $mCD45^+$ cells were sorted from PDX mice at the indicated points and seeded in methylcellulose and scored to colony forming units after 7 days. Cultures were dissolved in PBS, counted and 10^4 cells were re-seeded for passage 2 and passage 3.

Viability assays

Relative cell viability was assessed by % reduction O_2 in culture wells using the Alamar blue cell viability reagent (Life Technologies). Cells were seeded in 96 well plates at $2x10^5$ cells/ml and the indicated dose of drugs were added on top and incubated for 48 hours. Alamar blue reagent was added on top of cells, and cells were incubated for another 4 hours under the same conditions (37ºC, 5% CO_2). Plates were read on a spectramax plate reader (Biostars) at 570nm and 600nm and % reduction O_2 was calculated as per the manufacturer's instructions.

Flow Cytometry, apoptosis and cell cycle assays

Flow cytometry analysis was performed using a BD Fortessa flow cytometer (BD biosciences). Cells were prepared by washing in PBS + 1% FBS three times before staining in the same media with the indicated cell surface antibodies (resources table) for 1 hour at 4C. For apoptosis assays, cells were incubated with annexin V binding buffer in addition to the washing media (BD biosciences), washed three times in PBS + 1% FBS + 1x annexin V binding buffer and incubated with 0.1μg/ml DAPI prior to flow cytometry analysis. For cell cycle analysis, cells were washed three times in PBS + 1% FBS and fixed in BD fix/perm buffer (BD biosciences) for 20 minutes at room temperature. Cells were washed three times in BD perm/wash buffer + 0.1% Triton X-100 (BD biosciences) and incubated with intracellular antibodies, such as anti-Ki67, for 4 hours at 4C. Cells were washed three times in BD perm/wash buffer and 0.5 μg/ml DAPI was added for 15 minutes prior to analysis. For all flow cytometry, cells were initially identified based on forward and side scatter.

RNA extraction, reverse transcription and real time quantitative PCR (RT-qPCR)

Total RNA was isolated from patient samples after thawing, density centrifugation and T-cell depletion, using a RNeasy mini kit (Qiagen). Resulting RNA was reverse transcribed to produce cDNA using the Superscript III reverse transcriptase kit (Thermo Fisher Scientific) with oligoDT_{20} primers (Sigma Aldrich). RT-qPCR experiments were performed with an ABI-7500 FAST Thermal Cycler (Applied Biosystems) using SYBR Green (Thermo Fisher Scientific). RNA abundance was quantified by the Comparative CT method with two independent control genes (*GAPDH* and *B-ACTIN*, *GAPDH* presented). The CT values used for each patient sample were the result of three technical triplicates. Primers are described in the resources table.

RAC1/RHOA G-LISA assay

Analysis of RAC1/RHOA-GTP abundance was carried out using the RAC1/RHOA G-LISA assay as per the manufacturer's instructions (Cytoskeleton inc.). Control and CKS1i treated AML cells were lysed on ice with the provided lysis buffer for 10 minutes and centrifuged at 10,000g, 4°C, for 5 minutes. Protein was quantified and normalized with precision red protein reagent. Lysate, lysis buffer only or control protein was incubated with G-LISA wells at 4°C for 30 minutes with agitation. Wells were washed three times with wash buffer and primary antibody incubation was carried out at room temperature for 45 minutes with agitation. Wells were washed three times with wash buffer and secondary antibody incubation was carried out at room temperature for a further 45 minutes with agitation. HRP detection reagent was added to each well and incubated at room temperature for 20 minutes (RAC1) or 15 minutes at 37C (RHOA) in the dark followed by measurement at 490nm.

Supplementary Figures

Supplementary Figure 1.

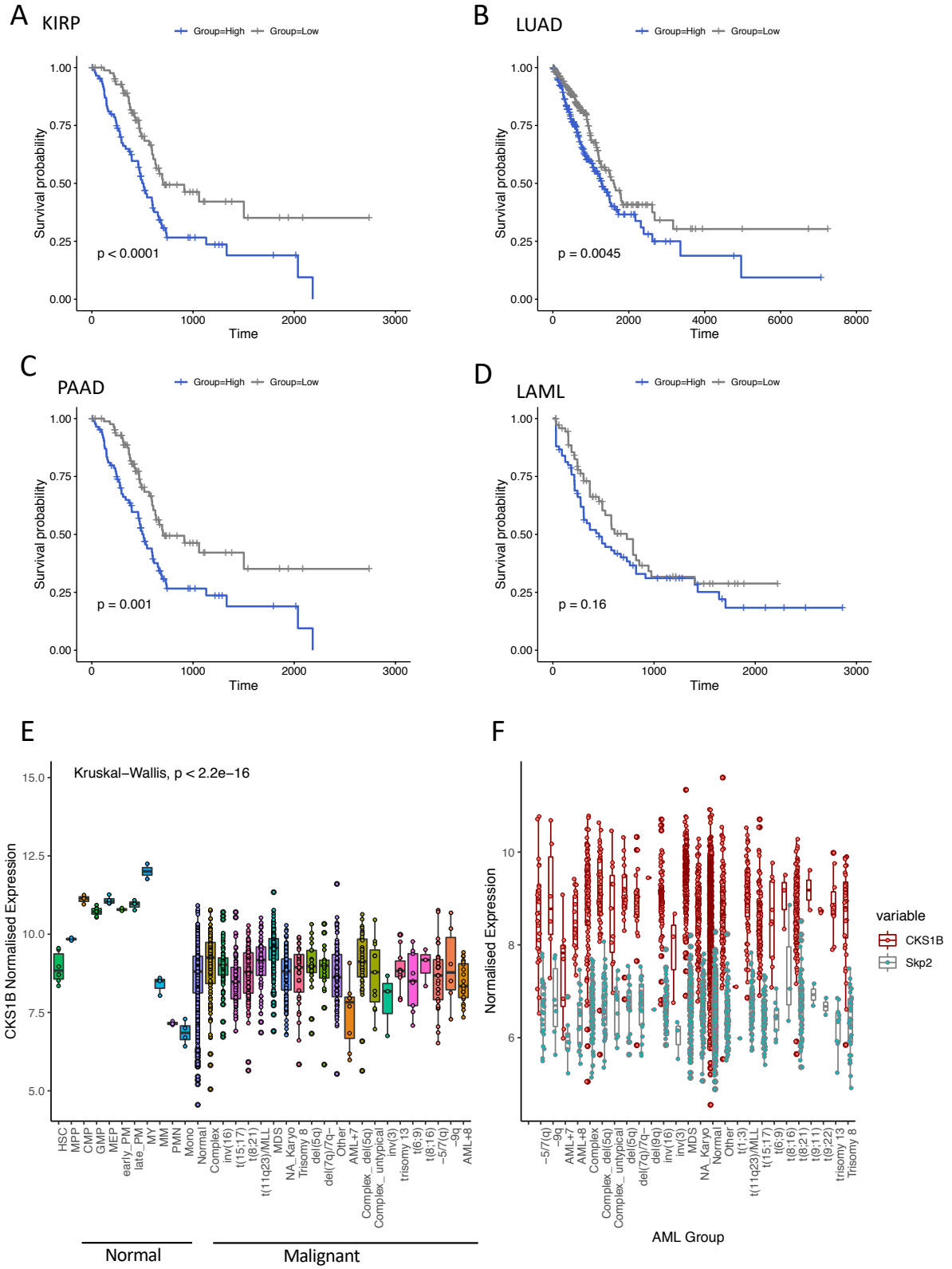

Supplementary Figure 1. Expression of *CKS1B* across publicly available datasets. A-D. Overall survival of TCGA patients stratified for *CKS1B* expression (50th percentile). Cohorts are as follows: KIRP = Kidney Renal Papillary Cell Carcinoma, LUAD = Lung Adenocarcinoma, PAAD = Pancreatic Adenocarcinoma, LAML = Acute Myeloid Leukemia. **E** *CKS1B* normalized expression and **F.** *SKP2* compared to *CKS1B* normalized expression of normal and malignant hematopoeitic cells obtained from Bloodspot.eu. Data sources: Human normal hematopoiesis (GSE42519), Human AML (GSE13159, GSE15434, GSE61804, GSE14468 and The Cancer Genome Atlas; TCGA).

Supplementary Figure 2.

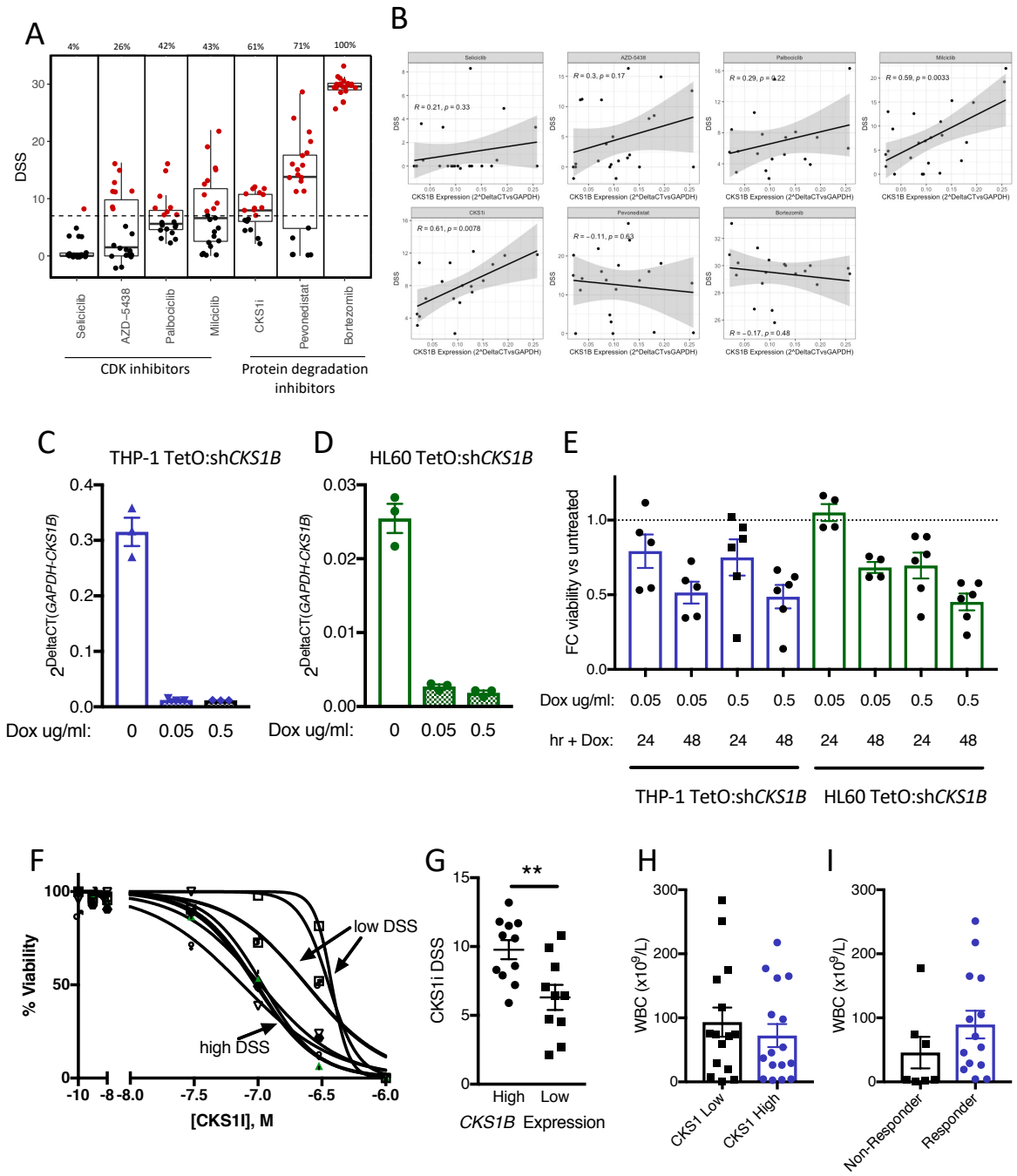

Supplementary Figure 2. Analysis of drug and genetic targeting of CKS1 in primary AML samples and AML cell lines A. Drug sensitivity score (DSS) for CDK

and protein degradation inhibitors in primary AML samples. Red indicates robust DSS (>7), percentage above indicates proportion of patients with robust response. **B.** Correlation between patient AML CKS1i drug sensitivity (DSS) and *CKS1B* expression for the indicated drugs. 95% confidence intervals presented. Pearson's correlation coefficient was calculated for correlation (R^2) and significance (*P*). Expression of *CKS1B* in **C.** THP-1 and **D.** HL60 cells transduced with TetO:shRNA:*CKS1B* in response to the indicated doses of doxycyclin after 24 hours. **E.** Fold change viability compared to uninduced control THP-1 (Blue) and HL60 (Green) cells transduced with TetO:shRNA:*CKS1B* in response to the indicated doses of doxycyclin for the indicated time points. **F.** Example dose dependent response curves for primary patient AML samples, indicating patient samples with high and low. **G.** CKS1i DSS grouped by *CKS1B* expression cut at the 50^{th} percentile. White blood cell counts ($x10^6$/L) of patients with AML comparing **H.** *CKS1B* high versus low expression and **I.** CKS1i responders versus non-responders. A Student's *t*-test was used to calculate significance of difference for all graphs unless otherwise stated. ** $P<0.005$.

Supplementary Figure 3.

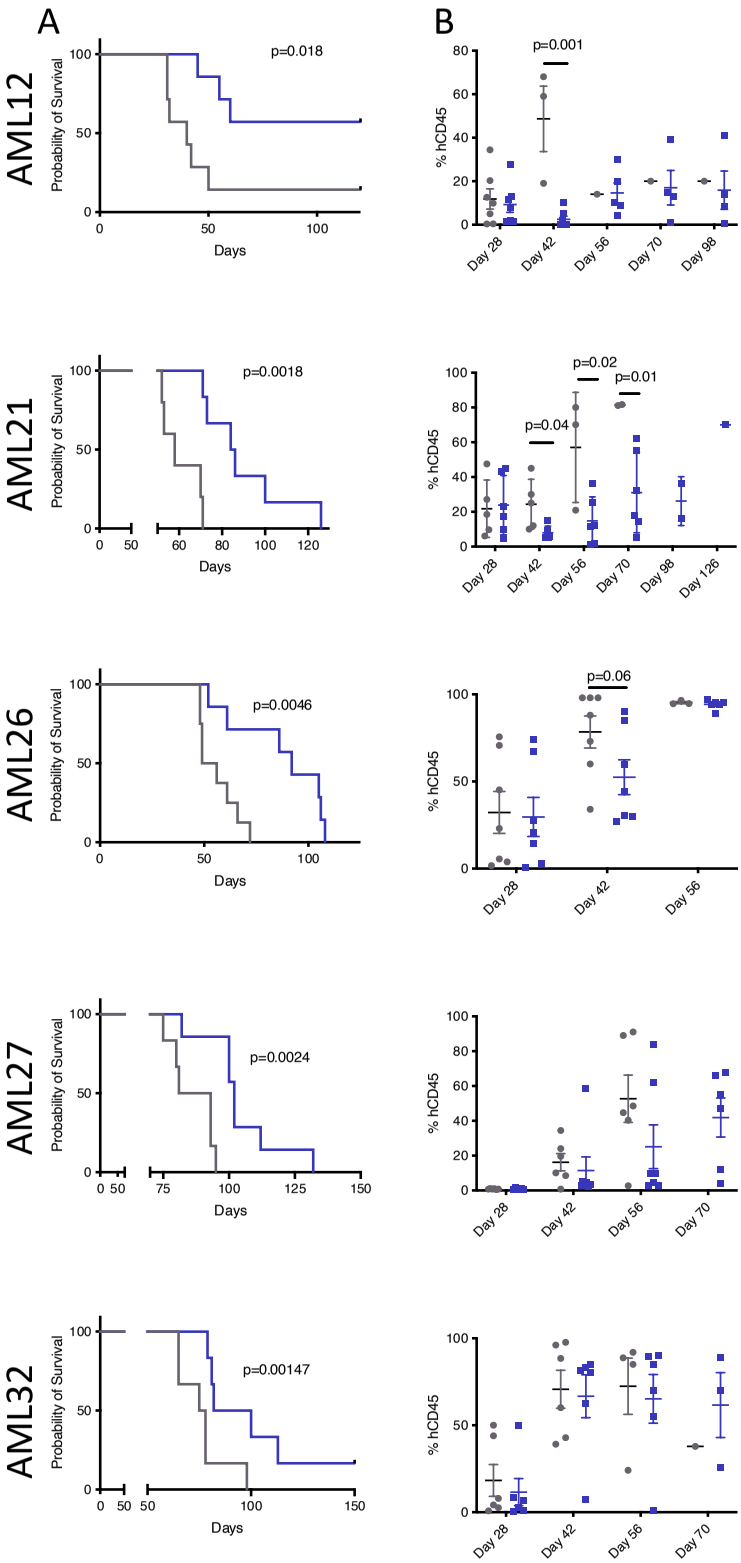

225

226

Supplementary Figure 3. Overall survival and bone marrow engraftment of patient derived xenografts. A. Kaplan Meier plots representing overall survival and **B.** Serial bone marrow aspirations for primary patient AML engrafted in NSG mice (Control = Grey, CKS1i treated = Blue, AML12 Control *n* = 7 CKS1i *n* = 7, AML21 Control *n* = 5 CKS1i *n* = 6, AML26 Control *n* = 7 CKS1i *n* = 7, AML27 Control *n* = 6 CKS1i *n* = 7, AML32 Control *n* = 6 CKS1i *n* = 6).

234

Supplementary Figure 4.

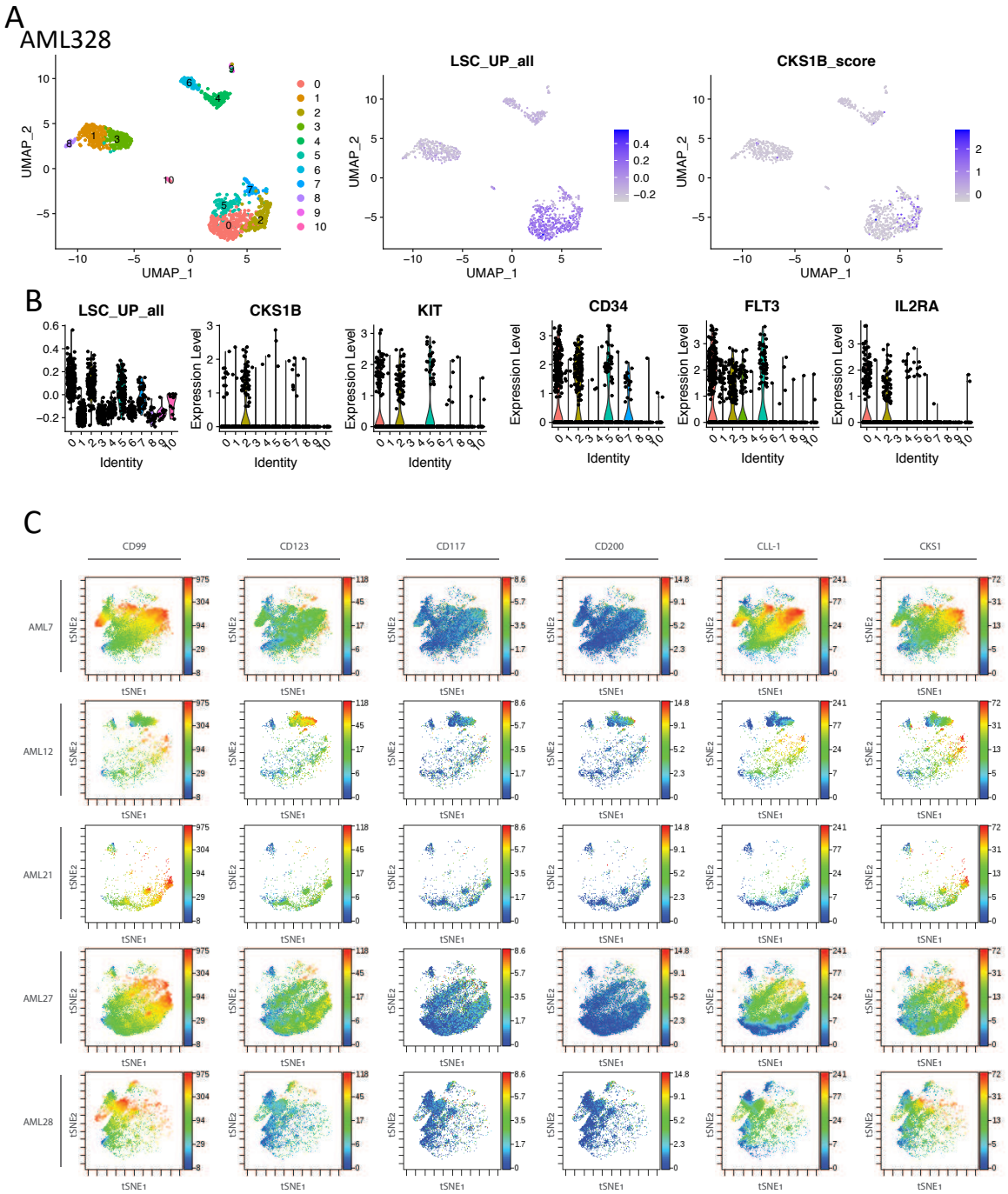

235

Supplementary Figure 4. Analysis of CKS1 expression in AML LSCs. A-B. Single cell RNAseq analysis for patient AML328 obtained from van Galen *et al.* (2019). Analyses present UMAP reductionality for cluster assignment, aggregated expression of “LSC up” gene score from Ng *et al.* (2016), *CKS1B* expression and violin plots for “LSC up” and individual genes. **C.** *t*-stochastic neighbour embedding of the indicated patients from CyTOF analyses. All markers were used for dimensionality reduction, key LSC cell surface markers and CKS1 are presented.

Supplementary Figure 5.

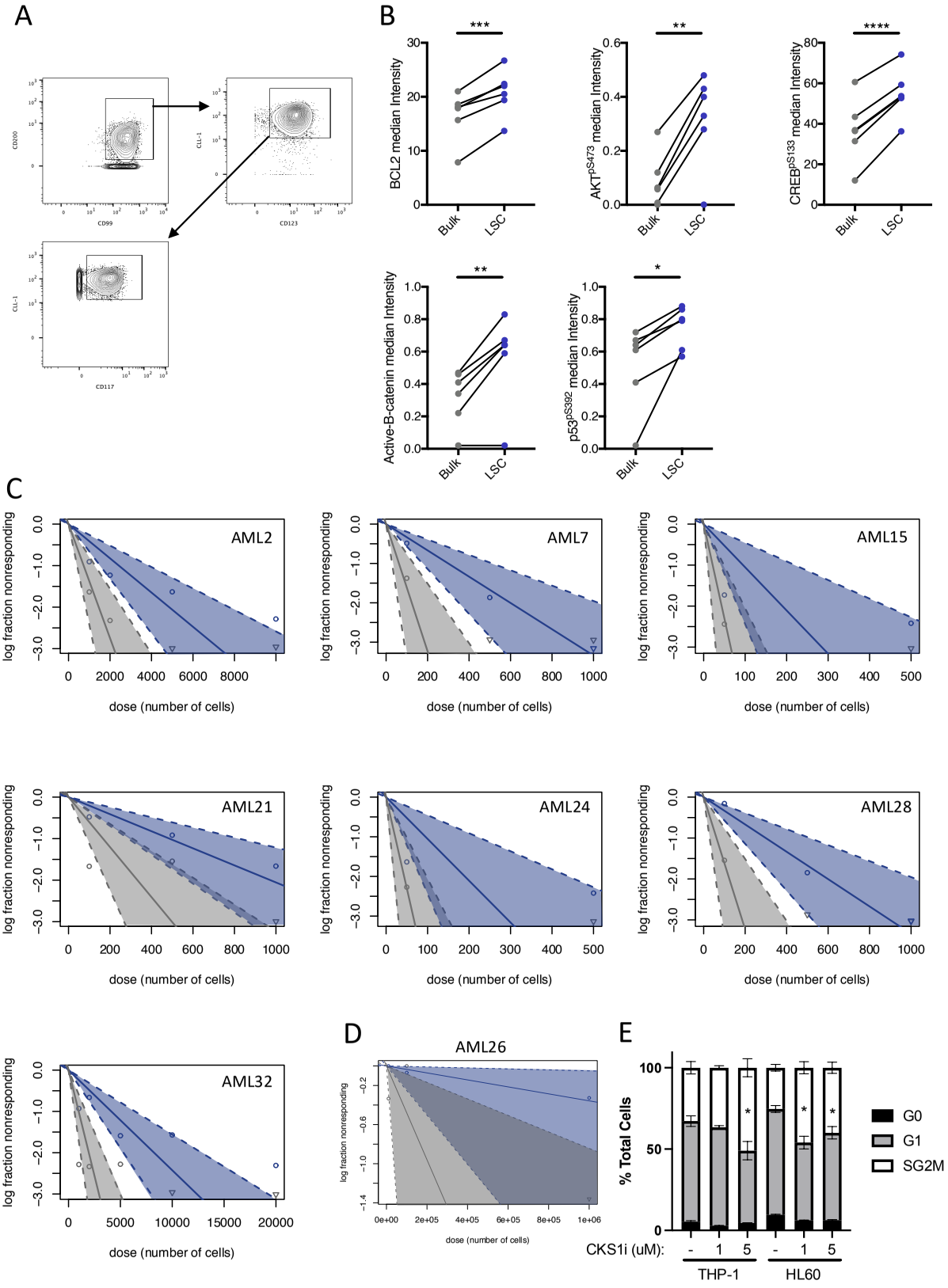

246

247

Supplementary Figure 5. Patient AML LSC response to CKS1i. A. Gating strategy for defining LSCs in bulk AML samples. Cells were gated for live, single cells and de-barcoded before example gating. **B.** Median intensity of the indicated proteins from CyTOF analyses of Bulk AML and LSCs. **C.** Graph of estimated L-LTC-IC frequency for the indicated patients control (grey) and treated with CKS1i (blue). **D.** Graph of estimated LSC frequency for AML patient 26 treated in the primary xenograft with control (grey) or CKS1i (blue). **E.** Cell cycle profiles of the indicated AML cell lines in response to CKS1i after 24 hours.

Supplementary Figure 6

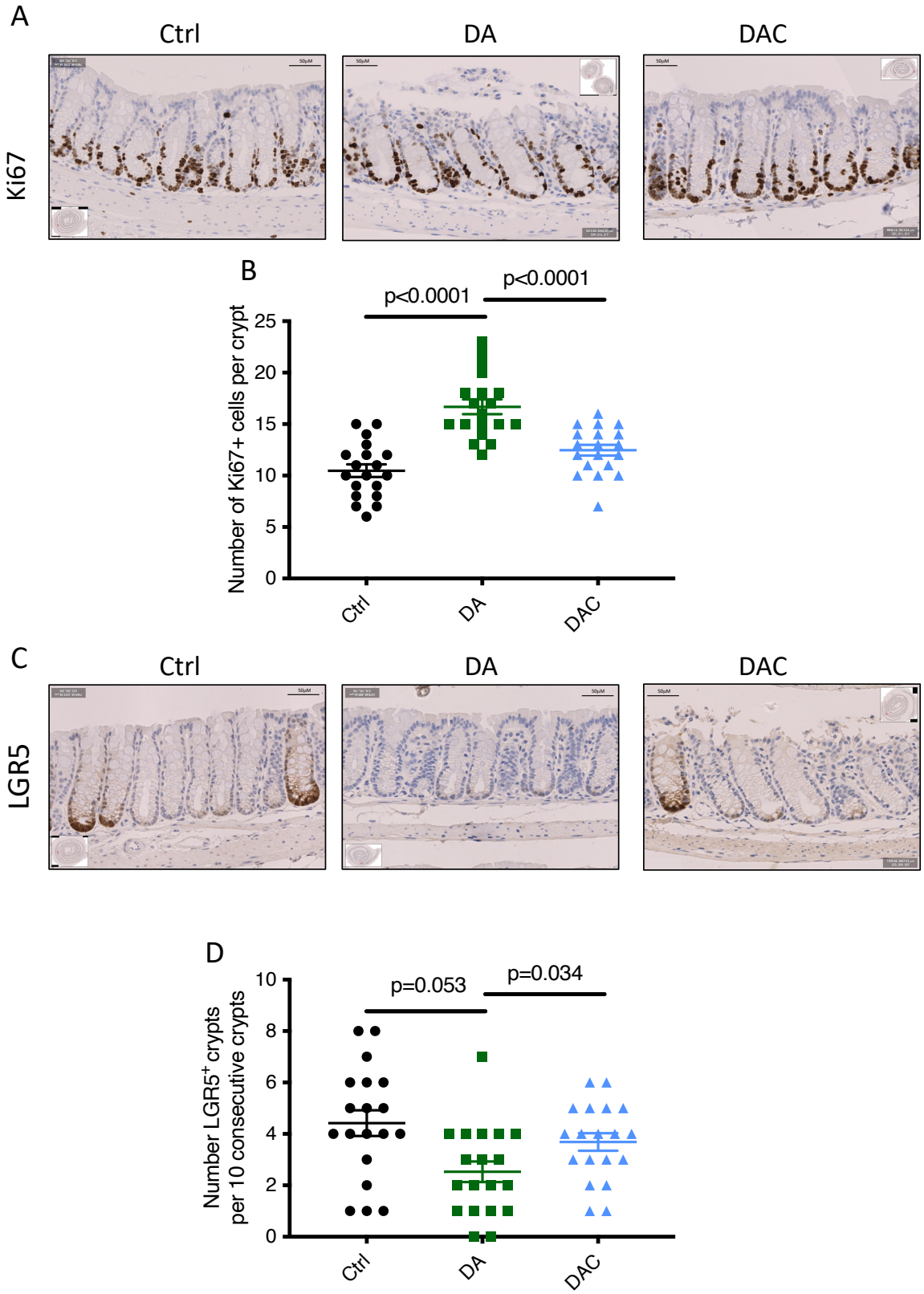

256

257

Supplementary Figure 6 Effect of combination chemotherapy on mouse intestinal crypts. A. Representative intestinal crypts stained with Ki67 and **B.** Number of Ki67 positive cells per crypt for the indicated treatments. **C.** Representative intestinal crypts stained for anti-GFP in LGR5-GFP mice and **D.** Number of LGR5 positive crypts per 10 consecutive crypts in intestinal preparations.

Supplementary Figure 7

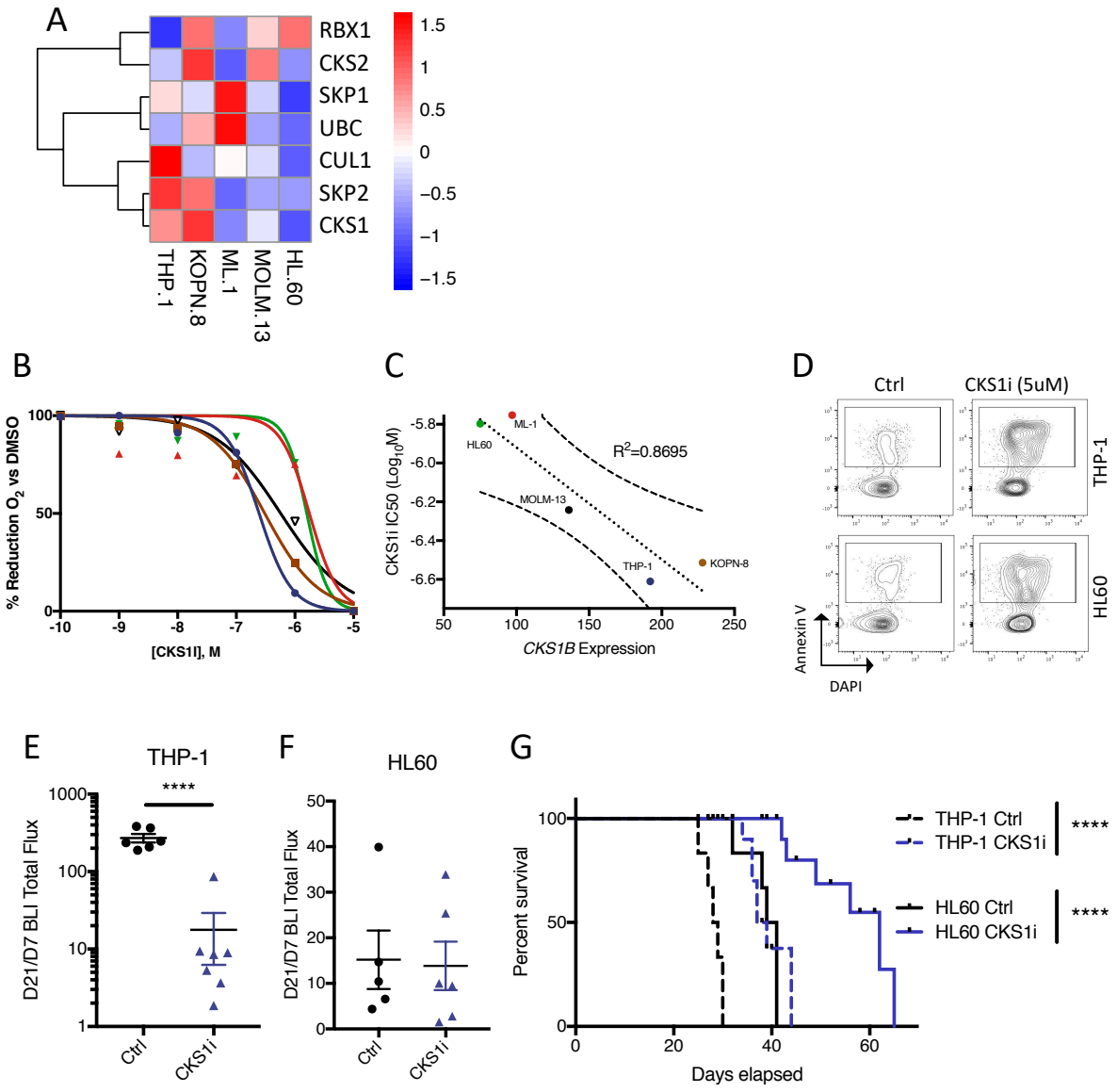

264
265

Supplementary Figure 7. AML cell line *CKS1B* expression dictates CKS1i sensitivity. A. Expression of key $SCF^{SKP2\text{-}CKS1}$ subunits in leukemic cell lines used in this study. Data presented are *z*-normalised (per gene) transcripts per million reads (TPMs) from the EBI Cell Line Expression Atlas. **B.** Percentage viability of AML cell lines cultured for 48 hours with indicated doses of CKS1i (*n*=3 for all cell lines on graph). **C.** Correlation between AML cell line CKS1i IC_{50} and *CKS1B* expression. 95% confidence intervals presented. Pearson's correlation coefficient was calculated for correlation (R^2). **D.** Representative FACS plots for induction of apoptosis in the indicated AML cell lines by presence of annexin V at the cell surface in response to CKS1i (5μM) at 48 hours. Fold change in vivo leukemic burden of **E.** THP-1 (Ctrl *n*=6, CKS1i *n*=7) and **F.** HL60 (Ctrl *n*=5, CKS1i *n*=6) cells day 21 (9 days post-CKS1i) versus day 7 (pre-CKS1i) expressed as bioluminescent total flux intensity. **G.** Overall survival of xenografts carrying THP-1 and HL60 cell lines control or treated with CKS1i. A Student's *t*-test was used to calculate significance of difference for all graphs unless otherwise stated. **** *P*<0.00005.

Supplementary Figure 8

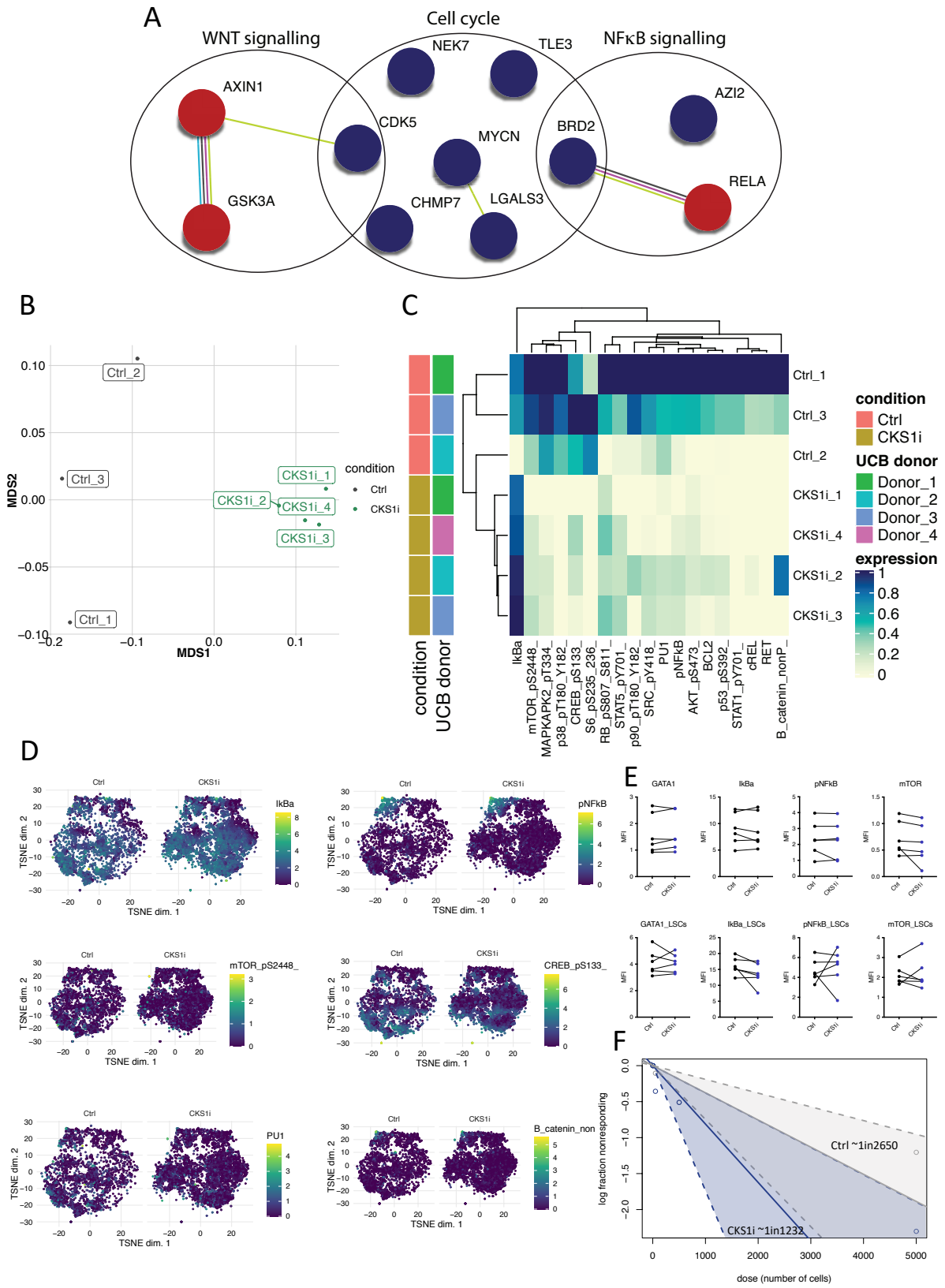

Supplementary Figure 8. Effect of CKS1i on healthy hematopoiesis. A. Key proteins differentially abundant in $CD34^+$ cells in response to CKS1i (Red = upregulated, Blue = downregulated). **B.** Pseudo-bulk-level multidimensional scaling (MDS) plot for all markers used in mass cytometry analyses. **C.** Unsupervised heatmap representing intracellular signalling markers in mass cytometric analyses *z*-scaled for each marker. **D.** *t*-distributed stochastic neighbor embedding for control vs CKS1i CyTOF samples with intensity scale for the indicated intracellular markers. **E.** Intracellular signalling components measured in primary AML bulk (top panel) or LSCs (bottom panel) post CKS1i treatment (1μM). **F.** LTC-IC estimated frequency of $CD34^+$ cells control (Grey) or treated with CKS1i (1μM, Blue).

Supplementary Figure 9

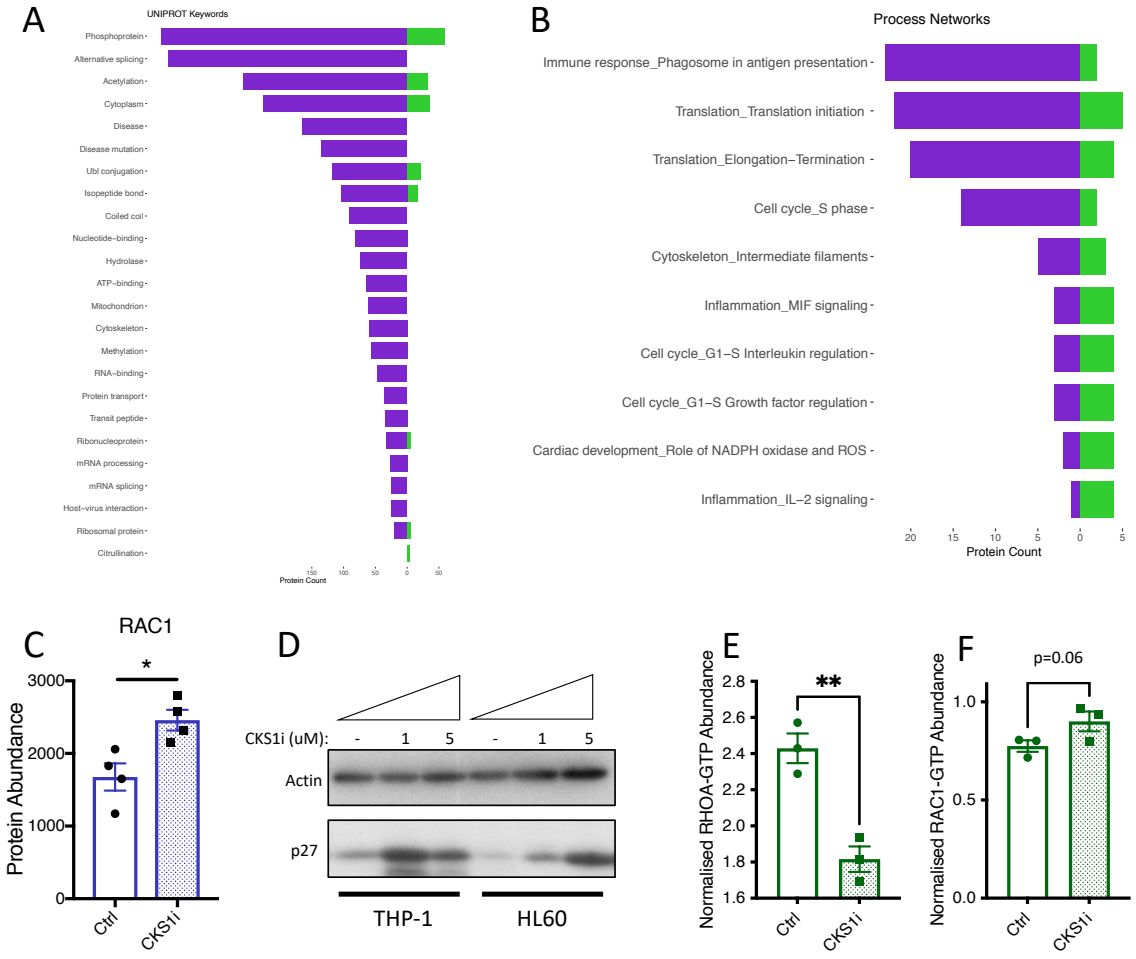

Supplementary Figure 9. Effect of CKS1i on AML cell lines. A. Uniprot keywords and **B.** Process networks from differentially abundant proteins in THP-1 (purple) and $CD34^+$ (green) cells. **C.** Abundance of RAC1 protein in THP-1 cells treated with CKS1i (1μM) from mass spectrometry analyses. **D.** Western blot for p27 in AML cell lines in response to the indicated doses of CKS1i after 24 hours. **E.** RHOA-GTP and **F.** RAC1-GTP abundance in HL60 cells treated with CKS1i (1μM). A Student's t-test was used to calculate significance of differences. * $P<0.05$, ** $P<0.005$.

Supplementary Figure 10

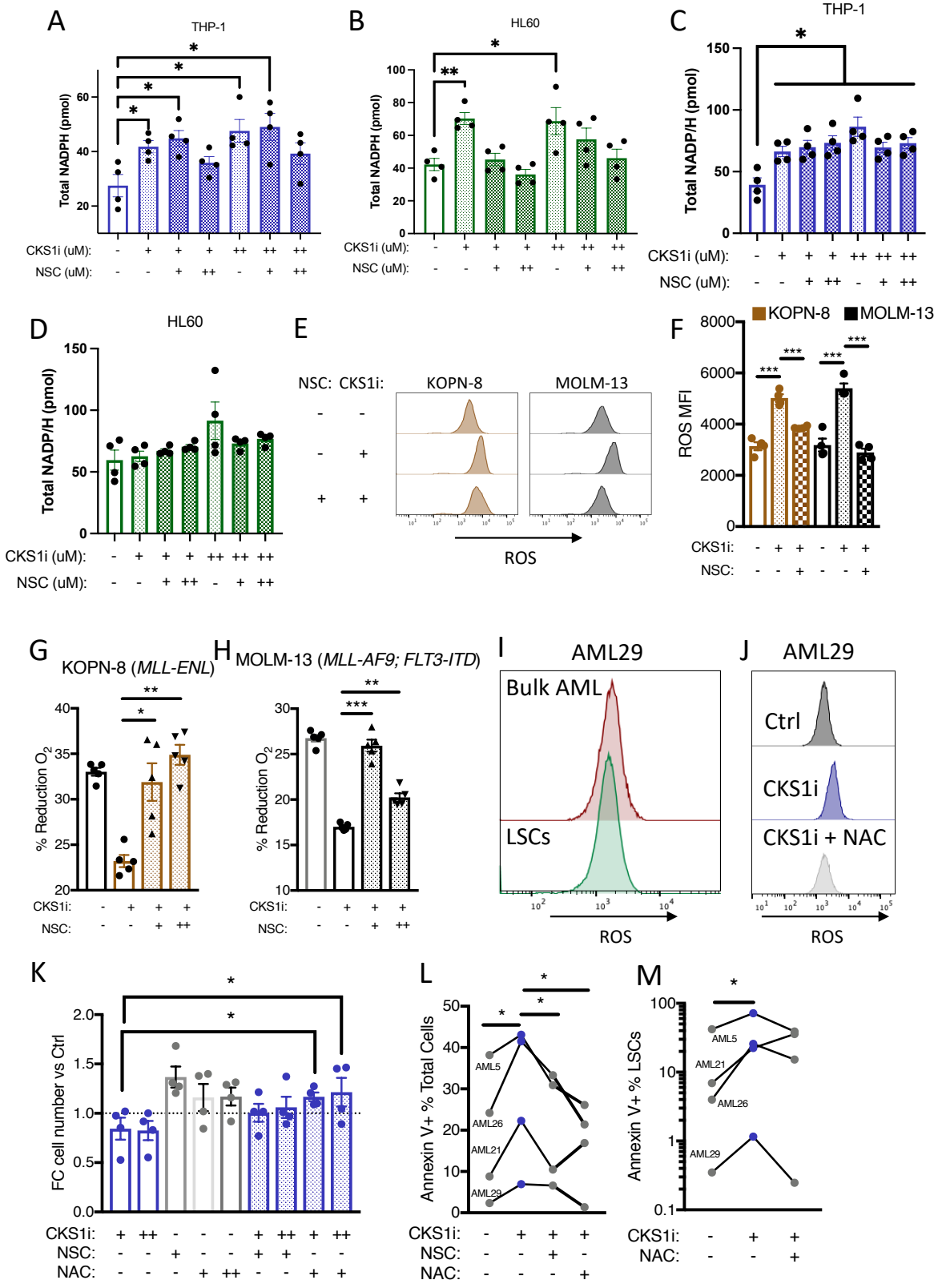

306

307

Supplementary Figure 10. CKS1i induces NADPH accumulation and lethal ROS in AML. Total NADPH (pmol) in **A.** THP-1 and **B.** HL60 cells treated for 8 hours with the indicated doses of CKS1i (+ = 1μM, ++ = 5μM) and NSC (+ = 0.1μM, ++ = 1μM). Total NADP/NADPH (pmol) in **C.** THP-1 and **D.** HL60 cells treated for 8 hours with the indicated doses of CKS1i (+ = 1μM, ++ = 5μM) and NSC (+ = 0.1μM, ++ = 1μM). **E.** Representative flow plots and **F.** Quantified mean fluorescence intensity of intracellular reactive oxygen species (ROS) in the indicated cell lines in response to CKS1i (+ = 1μM) and NSC (+ = 0.1μM) treatment (N=3 per cell line and treatment). Viability represented by percentage reduction O_2 of **G.** KOPN-8 and **H.** MOLM-13 cells in response to the indicated concentrations of CKS1i and NSC (N=5 per cell line and treatment, except THP-1 where N=6), CKS1i (+ = 1μM) and NSC (+ = 0.1μM, ++ = 1μM). **I.** Intracellular ROS measured in primary patient AML bulk vs LSC fraction. **J.** Intracellular ROS measured in primary AML cultured in control conditions, with CKS1i (1μM) or CKS1i + NAC (1μM + 1.25mM). **K.** Fold change absolute live cell number of patient AMLs compared to controls for the indicated treatments (CKS1i + = 1μM, ++ = 5μM, NSC + = 0.1μM, NAC + = 1.25mM, ++ = 2.5mM). Each point represents one primary patient AML sample. Percentage of annexin V positive cells of **L.** total primary patient AMLs and **M.** immunophenotypic LSCs with the indicated treatments (CKS1i + = 1μM, ++ = 5μM, NSC + = 0.1μM, NAC + = 1.25mM, ++ = 2.5mM). A Student's *t*-test was used to calculate significance of difference for all graphs * $P<0.05$; ** $P<0.05$; *** $P<0.005$.

Supplementary Figure 11

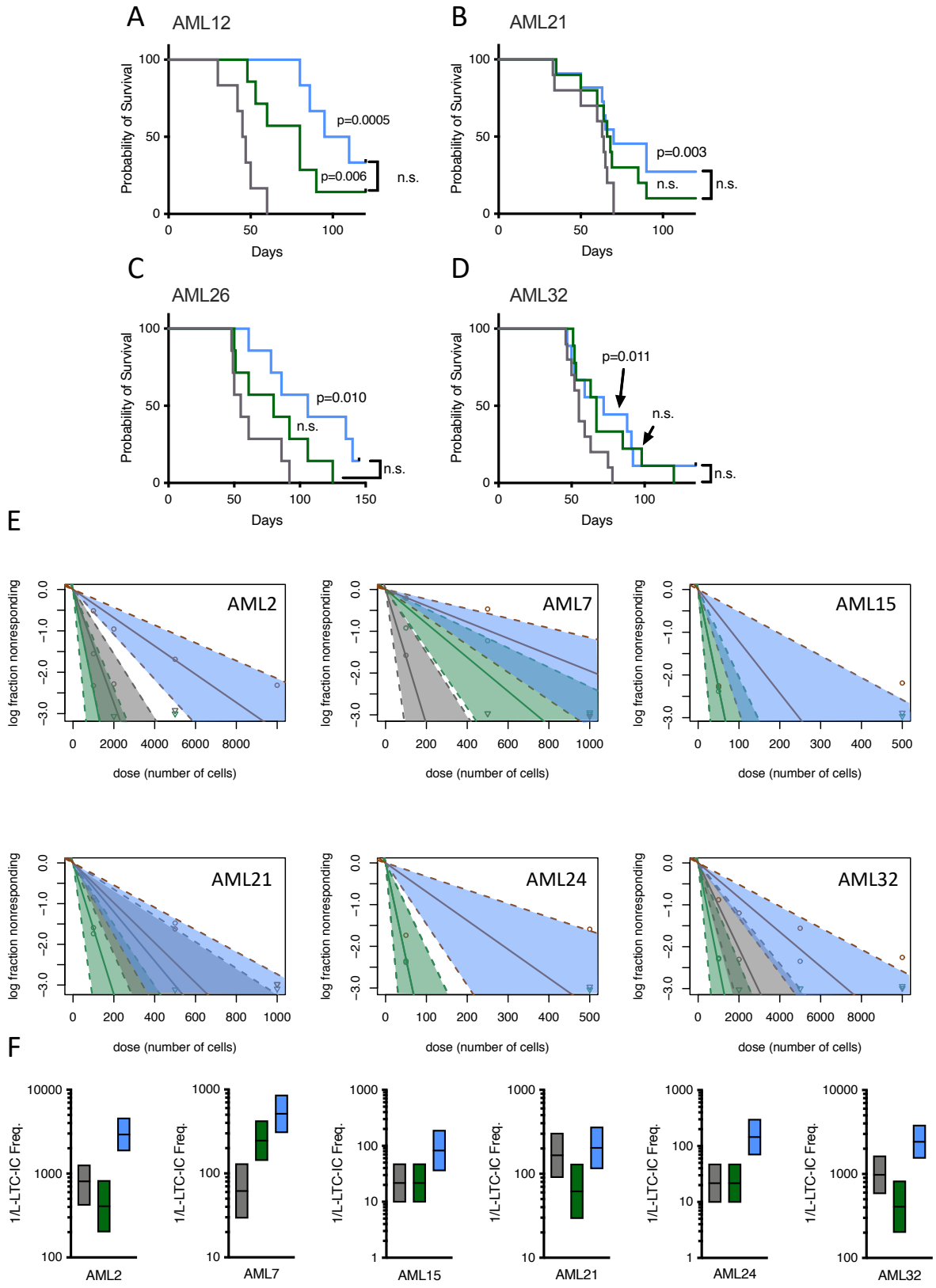

Supplementary Figure 11. In vivo and ex vivo response of patient AML samples to CKS1i. A-D. Kaplan Meier graphs for the indicated patient AML xenograft cohorts (Grey = control, green = DA, blue = DAC, AML12 control *n* = 6 DA *n* = 7 DAC *n* = 7, AML21 control *n* = 10 DA *n* = 10 DAC *n* = 11, AML26 control *n* = 7 DA *n* = 7 DAC *n* = 7, AML32 control *n* = 10 DA *n* = 9 DAC *n* = 9). **E.** Graph of estimated L-LTC-IC frequency for the indicated patients' control (Grey) and treated with DA (Green) or DAC (Blue). **F.** Calculated L-LTC-IC frequencies and confidence intervals by ELDA (Control = Grey, DA = Green, DAC = Blue).

Supplementary Figure 12

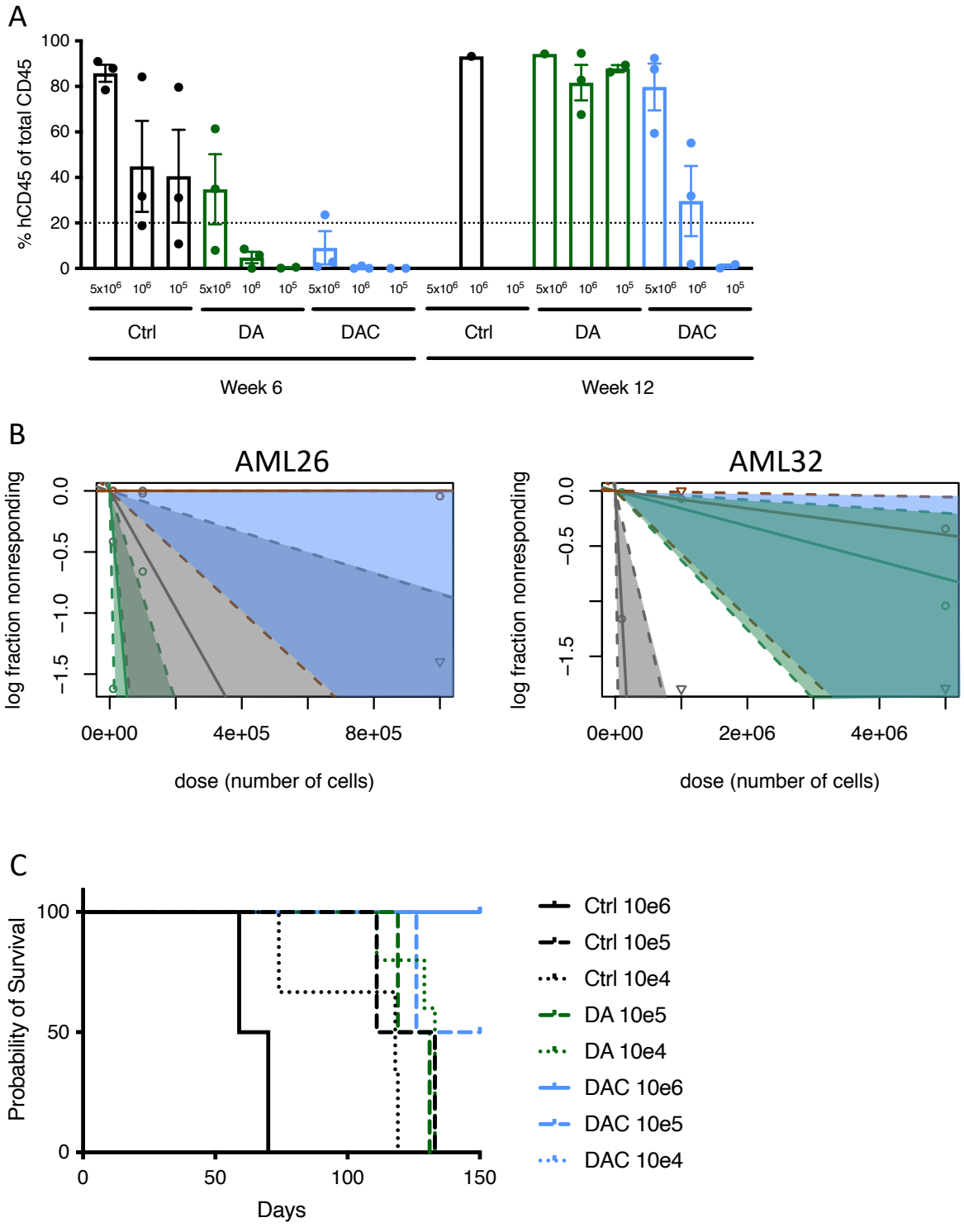

341

342

Supplementary Figure 12. Secondary transplantation of patient AML samples previously treated with chemotherapy. A. Percentage hCD45 bone marrow engraftment of AML32 engrafted in secondary mice at limiting dilution weeks 6 and 12 (Ctrl n = 3 per dose, DA 5x10^6 & 10^6 n = 3 per dose; 10^5 n = 2, DAC 5x10^6 & 10^6 & 10^5 n = 3 per dose). **B.** Graph of estimated LSC frequency for the indicated patients' control (Grey) and treated with DA (Green) or DAC (Blue). **C.** Overall survival of secondary transplantation mice from primary AML32 PDX control (Black) or treated with DA (Green) or DAC (Blue).

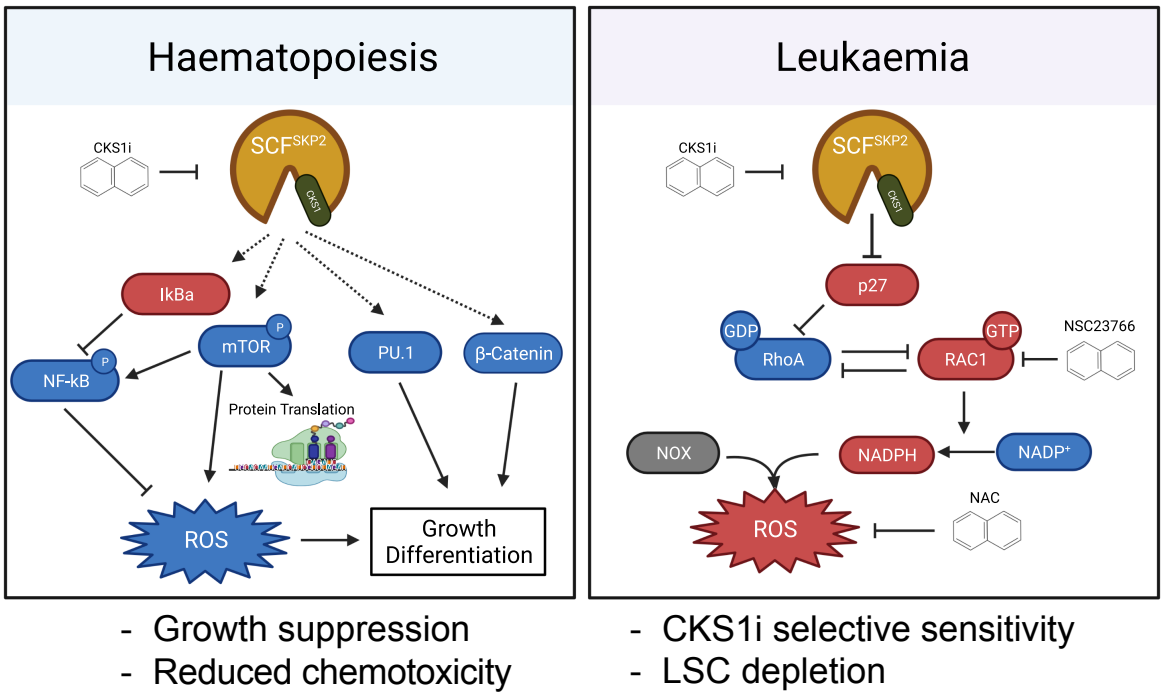

Graphical abstract. Model for mechanism of action for CKS1i in healthy hematopoiesis and leukemia.